JOURNAL OF GEOPHYSICAL RESEARCH, VOL. 106, NO. B7, PAGES 13,541–13,564, JULY 10, 2001

Upper crustal structure in Puget Lowland, Washington: Results from the 1998 Seismic Hazards Investigation in Puget Sound

Thomas M. Brocher,[1] Tom Parsons,[1] Richard J. Blakely,[1] Nikolas I. Christensen,[2] Michael A. Fisher,[1] Ray E. Wells,[1] and the SHIPS Working Group[3]

Abstract. A new three-dimensional (3-D) model shows seismic velocities beneath the Puget Lowland to a depth of 11 km. The model is based on a tomographic inversion of nearly one million first-arrival travel times recorded during the 1998 Seismic Hazards Investigation in Puget Sound (SHIPS), allowing higher-resolution mapping of subsurface structures than previously possible. The model allows us to refine the subsurface geometry of previously proposed faults (e.g., Seattle, Hood Canal, southern Whidbey Island, and Devils Mountain fault zones) as well as to identify structures (Tacoma, Lofall, and Sequim fault zones) that warrant additional study. The largest and most important of these newly identified structures lies along the northern boundary of the Tacoma basin; we informally refer to this structure here as the Tacoma fault zone. Although tomography cannot provide information on the recency of motion on any structure, Holocene earthquake activity on the Tacoma fault zone is suggested by seismicity along it and paleoseismic evidence for abrupt uplift of tidal marsh deposits to its north. The tomography reveals four large, west to northwest trending low-velocity basins (Tacoma, Seattle, Everett, and Port Townsend) separated by regions of higher velocity ridges that are coincident with fault-bounded uplifts of Eocene Crescent Formation basalt and pre-Tertiary basement. The shapes of the basins and uplifts are similar to those observed in gravity data; gravity anomalies calculated from the 3-D tomography model are in close agreement with the observed anomalies. In velocity cross sections the Tacoma and Seattle basins are asymmetric: the basin floor dips gently toward a steep boundary with the adjacent high-velocity uplift, locally with a velocity "overhang" that suggests a basin vergent thrust fault boundary. Crustal fault zones grow from minor folds into much larger structures along strike. Inferred structural relief across the Tacoma fault zone increases by several kilometers westward along the fault zone to Lynch Cove, where we interpret it as a zone of south vergent faulting overthrusting Tacoma basin. In contrast, structural relief along the Seattle fault zone decreases west of Seattle, which we interpret as evidence that the N-S directed compression is being accommodated by slip transfer between the Seattle and Tacoma fault zones. Together, the Tacoma and Seattle fault zones raise the Seattle uplift, one of a series of east-west trending, pop-up structures underlying Puget Lowland from the Black Hills to the San Juan Islands.

[1]U.S. Geological Survey, Menlo Park, California.

[2]Department of Geology and Geophysics, University of Wisconsin-Madison, Madison, Wisconsin.

[3]Uri S. ten Brink, U.S. Geological Survey; Thomas L. Pratt, U.S. Geological Survey; Robert S. Crosson, Department of Earth and Space Sciences, University of Washington; Kenneth C. Creager, Department of Earth and Space Sciences, University of Washington; Neill P. Symons, Sandia National Laboratories; Leiph A. Preston, Department of Earth and Space Sciences, University of Washington; Thomas Van Wagoner, Department of Earth and Space Sciences, University of Washington; Kate C. Miller, Department of Geological Sciences, University of Texas at El Paso; Catherine M. Snelson, Department of Geological Sciences, University of Texas at El Paso; Anne M. Tréhu, College of Oceanography, Oregon State University; Victoria E. Langenheim, U.S. Geological Survey; George D. Spence, School of Earth and Ocean Sciences, University of Victoria; Kumar Ramachandran, School of Earth and Ocean Sciences, University of Victoria; Roy A. Hyndman, Pacific Geoscience Centre; David C. Mosher, Atlantic Geoscience Centre; Barry C. Zelt, School of Ocean and Earth Science and Technology, University of Hawaii; and Craig S. Weaver, U.S. Geological Survey.

Copyright 2001 by the American Geophysical Union.

Paper number 2001JB000154.
0148-0227/01/2001JB000154$09.00

1. Introduction

The Puget Lowland of Washington is seismically active, and known or suspected crustal faults beneath the lowland include the Olympia, Tacoma, Seattle, Hood Canal, southern Whidbey Island, and Darrington-Devils Mountain faults (Figure 1). Several of these structures are inferred to offset Quaternary deposits, and at least one, the Seattle fault zone, has a history of late Holocene rupture [*Gower et al.*, 1985; *Atwater and Moore*, 1992; *Bucknam et al.*, 1992; *Johnson et al.*, 1994, 1996, 1999; *Nelson et al.*, 1999; *Sherrod*, 1998]. The major crustal fault zones bound the Tacoma, Seattle, and Everett basins (Figure 1), large geological features that may prolong and amplify the strong ground motions [*Brocher et al.*, 2000].

Extensive glacial deposits and forest cover make it difficult to determine the geometry of the sedimentary basins and locate the bounding crustal faults in the lowland. Connected waterways in the lowland permitted an areal geophysical experiment called Seismic Hazards Investigation in Puget Sound (SHIPS) to help better characterize the crustal architecture, basin geometry, and location of crustal fault zones. Other surveys in the Puget Sound designed to help locate possible crustal faults include (1)

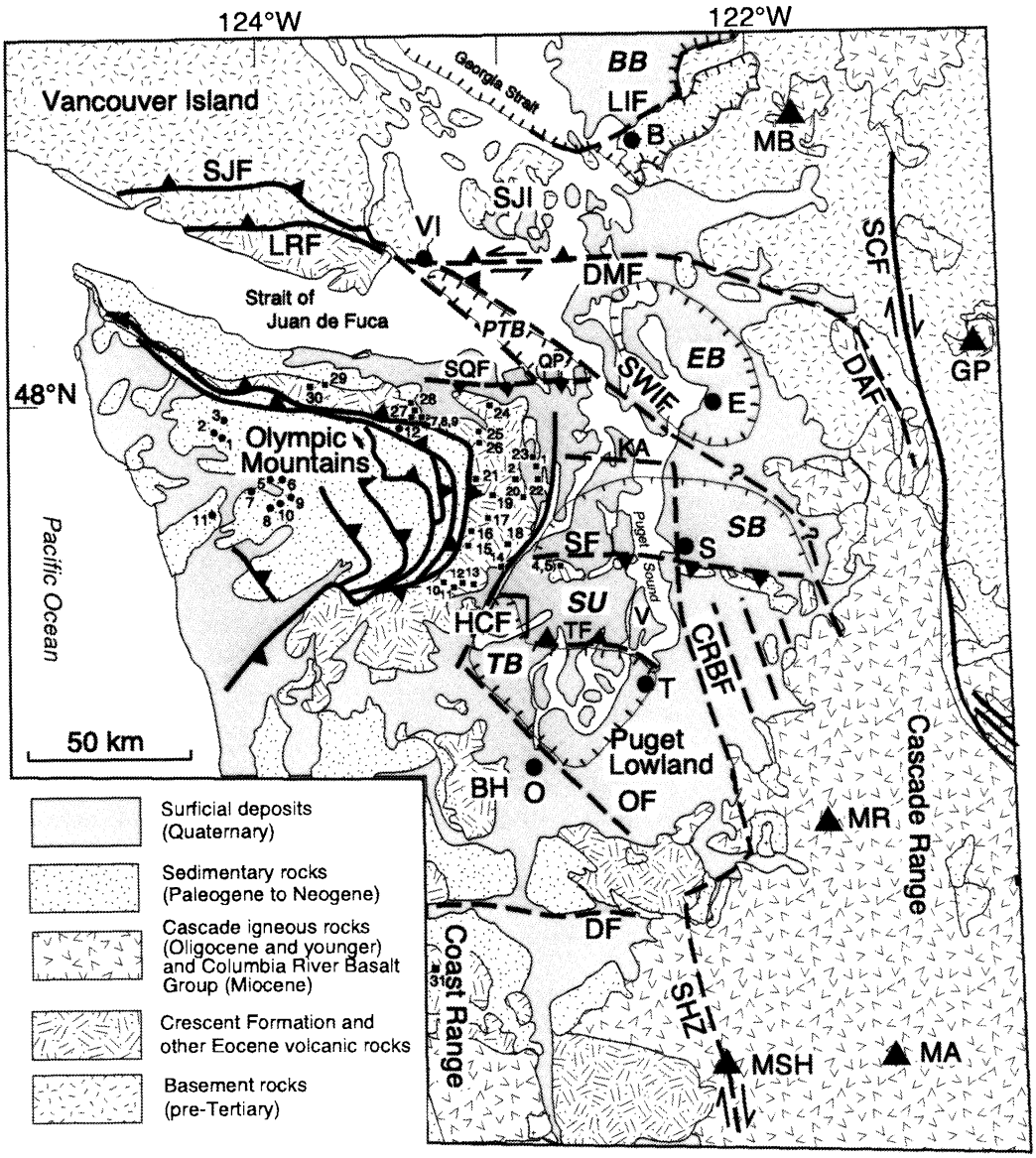

Figure 1. Schematic geologic map of northwestern Washington showing the Puget Lowland and flanking Cascade Range, Coast Range, and Olympic Mountains (modified from *Johnson et al.* [1999]). Numbered small solid circles and squares show locations of greywackes and mafic rocks, respectively, whose seismic velocities were measured in the laboratory. Abbreviations for cities are as follows: B, Bellingham; E, Everett; O, Olympia; S, Seattle; T, Tacoma; VI, Victoria. Abbreviations for faults (thick lines, dashed where uncertain), modern Cascade volcanoes (triangles), and other geologic features (basins are thin solid lines with ticks) are the following: BB, Bellingham basin; BH, Black Hills; CRBF, Coast Range boundary fault; DAF, Darrington fault; DF, Doty fault; DMF, Devils Mountain fault; EB, Everett basin; GP, Glacier Peak; HCF, Hood Canal fault; KA, Kingston Arch; LIF, Lummi Island fault; LRF, Leech River fault; MA, Mount Adams; MB, Mount Baker; MR, Mount Rainier; MSH, Mount Saint Helens; NS, Narrows structure; OF, Olympia fault; PO, Port Orchard; PTB, Port Townsend basin; QP, Quimper Peninsula; SB, Seattle basin; SCF, Straight Creek fault; SF, Seattle fault; SHZ, Saint Helens zone; SJI, San Juan Islands; SQF, Sequim fault; SU, Seattle uplift; SWIF, southern Whidbey Island fault; TB, Tacoma basin; TF, Tacoma fault.

aeromagnetic investigations [*Blakely et al.*, 1999] (R. J. Blakely et al., Location, structure, and seismicity of the Seattle fault zone, Washington, submitted to the *Geological Society of America Bulletin*, 2000, hereinafter cited as R. J. Blakely et al., submitted manuscript, 2000), (2) Light Detection and Ranging (LIDAR) topographic mapping [*Bucknam et al.*, 1999], (3) high-resolution seismic reflection surveys [*Johnson et al.*, 1999; *Mosher and Johnson*, 2000], and (4) GPS surveys of deformation rates and directions [*Miller et al.*, 1998; *Khazaradze et al.*, 1999].

Previous tomography studies of the Puget Lowland used sparse microseismicity (occurring largely well below the sedimentary basins) recorded by widely separated seismic stations [*Lees and Crosson*, 1990; *Lees and VanDecar*, 1991; *Symons and Crosson*, 1997]. The resolution of sedimentary basin structures by these earlier studies was limited by the fact that few stations were located within the basins. *Symons* [1998] demonstrated that the 1998 SHIPS experiment significantly enhanced the resolution of the basin geometries relative to these

earlier studies by providing densely spaced shots and dense recording within the basins.

This paper is one of several presenting tomography models for the Puget Lowland based on 1998 SHIPS data and is based solely on the 1998 SHIPS data. *Crosson et al.* [2000] used both regional microseismicity and the SHIPS data to calculate a regional tomography model for the middle and lower crust. U.S. ten Brink (written communication, 2000) presented a model for deformation along the Seattle fault in the Puget Sound based on SHIPS seismic reflection profiles and tomographic images. *Mosher et al.* [2000] interpret SHIPS seismic reflection profiles, and *Zelt et al.* [2001] interpret a SHIPS-derived tomography model from the Georgia basin in the Strait of Georgia.

2. Regional Geology/Tectonic Setting

The Puget Lowland is part of a seismically active interior forearc basin above the subducting Juan de Fuca plate that stretches from the Georgia Strait in Canada to Eugene, Oregon. Beneath the central Puget Lowland the basement consists of older Mesozoic terranes in the north and east juxtaposed against Cenozoic accreted terranes of the Washington and Oregon Coast Ranges. Mafic rocks of the Siletz terrane, including the Eocene Crescent Formation of Washington, the correlative Siletz River Volcanics of Oregon, and the Metchosin Formation in Canada underlie much of the Cascadia forearc [*Snavely et al.*, 1968; *Massey*, 1986; *Snavely and Wells*, 1996; *Tréhu et al.*, 1994]. Sutured to North America at ~50 Ma, these voluminous (5-25 km thick) submarine and subaerial basalts may represent an accreted oceanic island chain [*Simpson and Cox*, 1977; *Duncan*, 1982] or a hot spot-generated continental margin rifting event [*Wells et al.*, 1984; *Babcock et al.*, 1992]. Crustal refraction profiling indicates that the inferred thickness of the Siletzia volcanic block progressively thins from central Oregon to northern Washington [*Tréhu et al.*, 1994; *Parsons et al.*, 1999], where Crescent Formation basalt wraps around the Olympic accretionary complex. Although the location of the contact between Siletzia and older basement rocks probably lies along the Leech River and southern Whidbey Island faults [*Johnson et al.*, 1996], its location beneath Puget Sound is uncertain [*Finn*, 1990; *Symons*

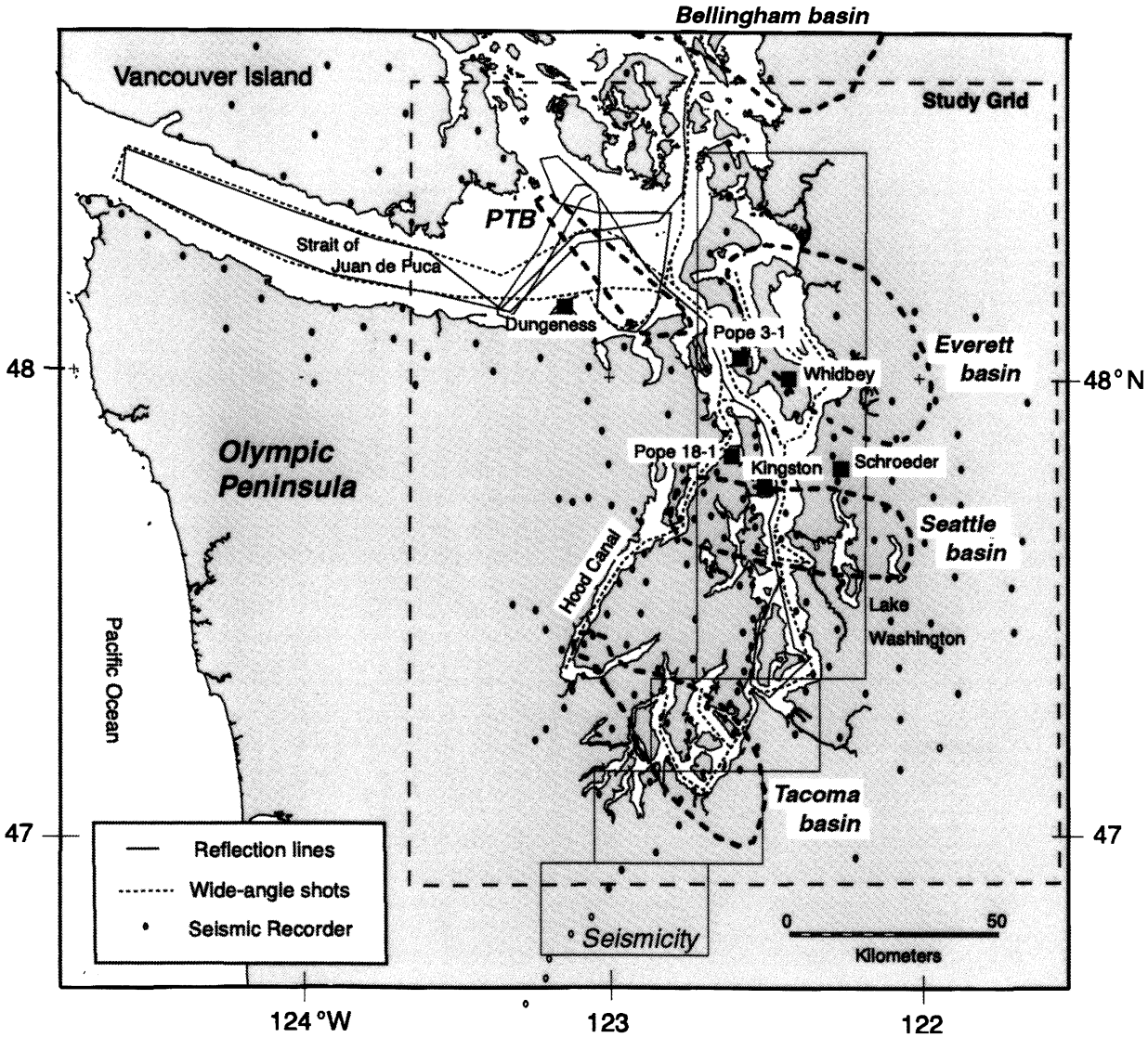

Figure 2. Map of Puget Lowland showing locations of Cenozoic basins, SHIPS seismic wide-angle and reflection lines (dashed and solid lines, respectively), and receivers (ellipses) providing first-arrival travel times used in our tomography study. Squares show locations of six industry boreholes having sonic velocity well logs. Rectangles show location of microseismicity plotted in Plate 8.

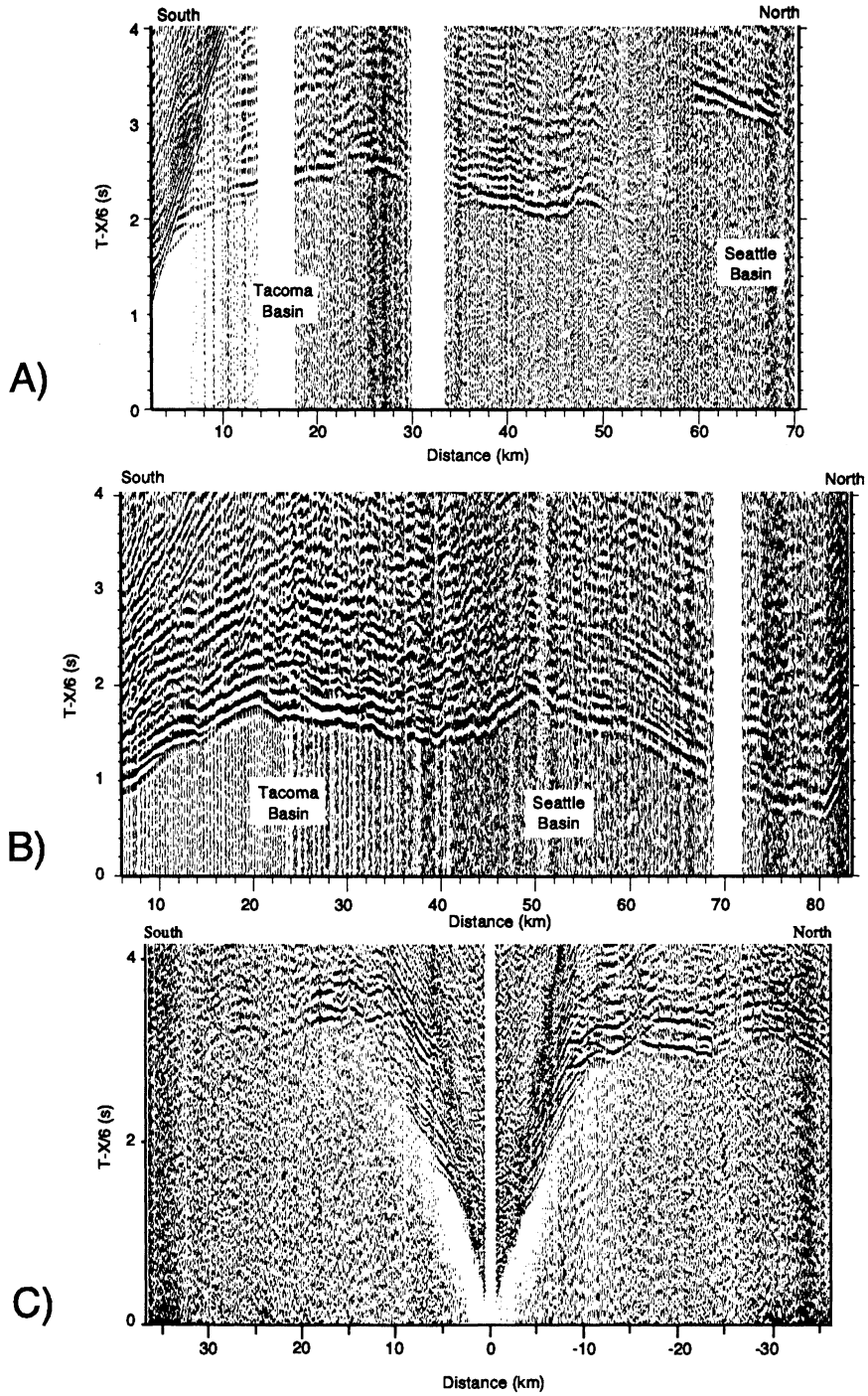

Figure 3. Three examples of wide-angle seismic data showing refractions from sedimentary rocks and the underlying basement as well as the large time delays introduced by the Tacoma and Seattle basins. (a) Data recorded at a station at the southern end of the Puget Sound (station. 8003) for a shot line in Puget Sound crossing the Seattle fault at a distance of 54 km. (b) Data recorded at a station at the southern end of Hood Canal (station 7007) for air gun shots along the canal. (c) Data collected using an ocean bottom seismometer in the Seattle basin for a shot line in Puget Sound.

and Crosson, 1997; *Moran et al.*, 1999; *Parsons et al.*, 1999; *Stanley et al.*, 1999].

Accreted sedimentary rocks in the core of the Olympic Mountains and along much of the Cascadia margin offshore have been thrust beneath basalt of the Siletz terrane along a terrane boundary fault that dips eastward beneath the Coast Range and the lowland [*Tabor and Cady*, 1978; *Brandon and Calderwood*, 1990; *Symons*, 1998; *Parsons et al.*, 1999; *Stanley et al.*, 1999; *Crosson et al.*, 2000]. Total crustal thickness of the Puget Lowland is ~45 km [*Miller et al.*, 1997; *Stanley et al.*, 1999].

Superimposed onto this convergent margin framework is a series of E-W trending folds, thrust faults, uplifts, and basins that form a narrow (90 km), N-S trending belt in the lowland that reflects several millimeters per year of north-south directed

shortening related to the oblique plate convergence [*Johnson et al.*, 1994; *Pratt et al.*, 1997; *Wells et al.*, 1998; *Khazaradze et al.*, 1999]. From south to north the main basins include the Tacoma, Seattle, Everett, and Bellingham basins (Figure 1: TB, SB, EB, and BB). This series of E-W elongated basins is evident in gravity data, oil industry test wells, and seismic reflection lines [*McFarland*, 1983; *Finn et al.*, 1991; *Johnson et al.*, 1994; *Pratt et al.*, 1997]. From the standpoint of earthquake hazard, one of the most important of the thrust faults in the Puget Lowland is the Seattle fault, whose E-W trend through Seattle is interpreted from high-resolution seismic lines and aeromagnetic data and which is associated with seismicity and paleoseismic evidence for Holocene offset [*Yount and Gower*, 1991; *Bucknam et al.*, 1992; *Johnson et al.*, 1999; *Weaver et al.*, 1999; R. J. Blakely et al., submitted manuscript, 2000]. Estimates from seismic reflection profiles of the total structural relief on the Seattle fault range from 8 to 9 km [*Johnson et al.*, 1994].

In terms of number of earthquakes, crustal seismicity in the Cascadia forearc of Washington and Oregon and southwestern British Columbia is concentrated in the Puget Lowland, although the 1872 event in the northeastern Cascades gives that region the greatest historic moment release [*Ludwin et al.*, 1991]. Tomography studies based on SHIPS data and local earthquakes indicate that the crustal seismicity occurs within the strong mafic rocks of the Crescent Formation and that the Benioff zone earthquakes occur within the oceanic crust of the subducting Juan de Fuca plate [*Stanley et al.*, 1999; *Crosson et al.*, 2000].

3. Field Work, Data Reduction, and Data Analysis

In March 1998, SHIPS participants conducted onshore-offshore wide-angle and multichannel seismic (MCS) reflection profiling throughout the Puget Lowland using an air gun array (Figure 2). The total volume of the air gun array varied between 110.3 L and 79.3 L depending on whether wide-angle or MCS data were acquired. Wide-angle profiling was conducted throughout the study region, even in narrow waterways such as the Hood Canal and Lake Washington where the multichannel seismic streamer could not be towed [*Fisher et al.*, 1999]. MCS profiling was performed in Puget Sound, the Strait of Juan de Fuca, and Georgia Strait (Figure 2). Air gun shot point locations and times accurate to a millisecond were determined from GPS navigation and GPS time recorded on the ship.

The air gun shots were recorded by a temporary array of 210 seismographs deployed onshore and on the floor of Puget Sound (Figure 2) [*Brocher et al.*, 1999]. All seismographs recorded the vertical geophone component, and 75 of the 210 seismographs recorded two horizontal geophone components. Shots recorded by the permanent Pacific Northwest Seismic Network stations are not included in this analysis.

The quality of the wide-angle data obtained during SHIPS is highly variable, although most stations provided useful data to source-receiver offsets of at least 40-50 km. At bedrock sites remote from urban centers, first arrivals can be observed to ranges up to 200 km. On the other hand, few interpretable data were recorded at some of the soft soil sites in urban or suburban localities.

The Tacoma and Seattle basins introduce a significant difference in the delay times of first arrivals produced along shot lines in Puget Sound versus Hood Canal (Figures 3a and 3b). In Puget Sound, travel time delays produced by the Seattle basin exceed 1 s. An example of the ocean bottom seismometer (OBS) data recorded from air guns shots in Puget Sound (Figure 3c) shows that first arrivals recorded to ranges of 15 km represent refractions from the sedimentary rocks filling Seattle basin. At ranges beyond 15 km the first arrivals represent refractions from within the rocks of the Crescent Formation underlying the Seattle basin.

4. Travel Time Inversion for the Upper Crustal Velocity Structure of Puget Lowland

4.1. Travel Time Data

A total of 977,000 *P* wave first-arrival travel times from controlled sources were included in our velocity modeling. Almost all of the travel times were from SHIPS; <1000 were from a 1991 seismic refraction study located along the eastern margin of the Puget Lowland [*Miller et al.*, 1997]. We conservatively estimate picking errors to be 100 ms (one cycle at 10 Hz). All arrivals used for inversion were refractions from the upper crust generally at source-receiver offsets <100 km. The SHIPS data were acquired with a shot spacing between 50 and 150 m and a receiver spacing of 5-15 km. The 1991 seismic refraction data were acquired with a shot spacing of 30 km and a receiver spacing of 600 m. The absence of deeper sources and longer offsets limit the deeper ray coverage and resolution of the model.

4.2. Velocity Modeling Methods

To determine the crustal velocities, we applied the three-dimensional (3-D) tomographic technique of *Hole* [1992] and followed the same procedures as detailed by *Parsons et al.* [1999]. This technique applies a finite difference solution to the eikonal equation (*Vidale* [1990], updated by *Hole and Zelt* [1995]) to calculate first-arrival times through a gridded slowness model. An iterative nonlinear inversion is performed as a back projection along ray paths determined from the forward modeling step.

4.3. Resolution of Tomography Model

We used hit counts to determine ray coverage and checkerboard tests to estimate the spatial and velocity resolution of the solution [*Humphreys and Clayton*, 1988] (Plate 1). Because all of our sources are located at the surface, maximum hit counts decrease with depth as the ray coverage becomes more uniform. Deeper than 13 km the hit counts decrease sharply, and for this reason we have chosen not to interpret the model below 11 km. Ray coverage is best in the central Puget Lowland, between the shot lines in Hood Canal and Lake Washington. The hit counts shown in Plate 1 are most uniform in the depth range of 3-9 km, where locally they exceed 5000 rays per km^3 and generally exceed 100 rays per km^3. For this reason we believe that the upper 9 km of the model is the best imaged.

The checkerboard tests reveal that the horizontal and relative velocity resolution varies with depth. The checkerboard tests were conducted by calculating synthetic travel time picks between all the source and receiver locations through a horizontally layered model of variable sized squares, 5 km x 5 km, 10 km x 10 km, 15 km x 15 km, and 20 km x 20 km. Each layer contained squares with velocities (alternating in both horizontal directions) that differed by 0.5 km/s (Plate 1). Although the velocities increased with depth, the 0.5 km/s checkerboard difference was maintained within each layer. Larger velocity contrasts between squares would be even more

resolvable than the 0.5 km/s contrast that we tested but might provide an unrealistically optimistic view of the resolution of the data. (In the resulting SHIPS tomography model, however, large velocity contrasts up to 1.5 km/s were imaged, suggesting that the horizontal resolution is better than the formal results presented below.) Note that because we apply a smoothing filter, described below, square corners are not recoverable in these checkerboard tests. We tested the model resolution only for models in which velocities increased with depth.

The checkerboard tests indicate that individual squares having horizontal dimensions of 15-20 km are generally resolvable. In addition, they indicate that because our data acquisition geometry was not uniform, the resolution is dependent on the location of the square in the model (Plate 1). Tests shown in Plate 1 show a generally increasing ability to resolve the squares as the horizontal length of the square is increased from 10 km by 10 km to 20 km by 20 km. Resolution generally peaks at 3-5 km depth and decreases with depth below 7 km. At 11 km depth and below the checker pattern is generally difficult to see (Plate 1), making results from these depths less reliable. Squares having horizontal dimensions of 5 km by 5 km are generally not resolvable because of the smoothing filter we applied and the average station spacing. At horizontal dimensions of 10 km by 10 km the squares can just be resolved but there is prominent streaking along the diagonals of the squares. At horizontal lengths of 15 km by 15 km the squares are generally resolvable, but streaks remain where there are only sources or receivers within the square but not both; this is true especially on eastern and northern sides of the model. Finally, at horizontal lengths of 20 km by 20 km the squares are generally resolvable and have close approximations to the correct velocities, but streaking remains in the northwest corner of the model. These dimensions are smaller than the lateral dimensions of the basins and uplifts that we seek to image.

During tomographic inversions it is important to scale the size of the horizontal smoothing filter dimensions appropriately to the input travel time data. On the basis of the distribution of seismic sources we sought to resolve velocity anomalies >10 km across the lateral dimensions and >2 km thick in the vertical dimension. We thus applied a 5 km wide by 1 km high smoothing filter during the final iteration, which yielded a RMS travel time misfit of 0.09 s. A smaller RMS misfit could be achieved but would require reducing the model smoothness below the appropriate scale for the input data coverage, resulting in an artificially detailed velocity model. The tomography model is presented in horizontal slices and vertical cross sections (Plates 2-4).

4.4. Accuracy of Shallow Velocities From Borehole Logging

Six deep industry boreholes in our study area provide sonic velocity logs (Figure 2). Comparison of the tomography model to these sonic velocity logs suggests that the shallow (upper 3 km) velocities are generally well recovered near the center of the model (Figure 4). This comparison shows that the velocity structure in the upper 3 km of the model matches the data from four of the six boreholes to within 0.2 to 0.3 km/s, particularly for the sedimentary rocks in the Oligocene Blakeley Formation filling the Seattle basin. The greatest misfit occurs at the Pope and Talbot 3-1 and Dungeness Spit 1 wells at the northern end of the tomography model in regions having sparse receivers. We cite the close agreement of the tomography model and sonic log hole data in the middle of the model as evidence that the vertical resolution of the SHIPS tomography model there is close to a kilometer. Thin (<300 m thick) layers of high-velocity Crescent Formation in the Socal Whidbey 1 and Pope and Talbot 18-1 boreholes were too thin to be resolved by the tomography method (Figure 4).

4.5. Accuracy of Basement Velocities in the Olympic Peninsula

Laboratory-determined velocities for 40 basement rocks outcropping in the Olympic Peninsula also permit an assessment of the tomography model (Plate 5). The greywackes were taken from the accretionary wedge of the Olympic core complex; the 29 mafic samples are mainly basalts from the Crescent Formation (Figure 1). Samples were field oriented by their bedding and flow structure. Velocities were measured in a hydrostatic pressure apparatus at room temperature using a pulse transmission technique described by *Christensen* [1985]. The laboratory data in Plate 5 are uncorrected for increasing temperature in the crust, which can significantly lower the velocities in the lower crust (corrections are approximately –0.02 to –0.06 km/s per 100°C increase in temperature [*Christensen*, 1979]). Mean *P* wave velocities for the two different rock suites at almost all confining pressures differ by at least 1 km/s: even the standard deviations of the velocities for the two suites are distinct (Plate 5).

The 6.3-6.6 km/s *P* wave velocity at 6 km depth imaged by the tomography along the Olympic Peninsula (Plate 2) compares favorably with the laboratory measurements of the Crescent Formation basalts at 200 MPa (Plate 5). Similarly, the 5.5-6.0 km/s *P* wave velocity of the rocks in the Olympic core complex (Plate 2), lies in the range of the laboratory measurements for the Olympic Peninsula greywackes (Plate 5). This comparison together with the comparison to the sonic logs in Figure 4 suggests that the tomography velocities may be accurate to 0.2 to 0.3 km/s over large portions of the model. However, our interpretation of the tomography model is largely based on the spatial pattern of the velocity anomalies rather than on their absolute value.

5. SHIPS Tomography Results

Before discussing the tomography model in detail we highlight a few of its key features. In the upper 3 km, the seismic

Plate 1. Resolution tests of the tomography models. (a) Ray coverage diagrams at 3 km, 7 km, and 11 km showing hit counts. (b) Checkerboard test for 10 km by 10 km squares. (c) Checkerboard test for 15 km by 15 km squares. (d) Checkerboard test for 20 km by 20 km squares. For all the checkerboard tests the initial velocities at 3 km were 5.25 and 5.75 km/s, the initial velocities at 7 km were 6.05 and 6.55 km/s, and the initial velocities at 11 km were 6.55 and 7.05 km/s. White grid lines show boundaries of the checkers. Fault zones (dotted white lines) are from *Johnson et al.* [1994, 1996, 2001] and R. J. Blakely et al. (submitted manuscript, 2000). Location of the Tacoma fault zone is modified from *Gower et al.* [1985]; abbreviations for faults are as for Figure 1. Black regions were not imaged by the tomography study. Thin black lines show shorelines; inverted white triangles show receiver locations; thin white lines show ship tracks. Velocity scale bar differs for each map. PLU, Port Ludlow uplift.

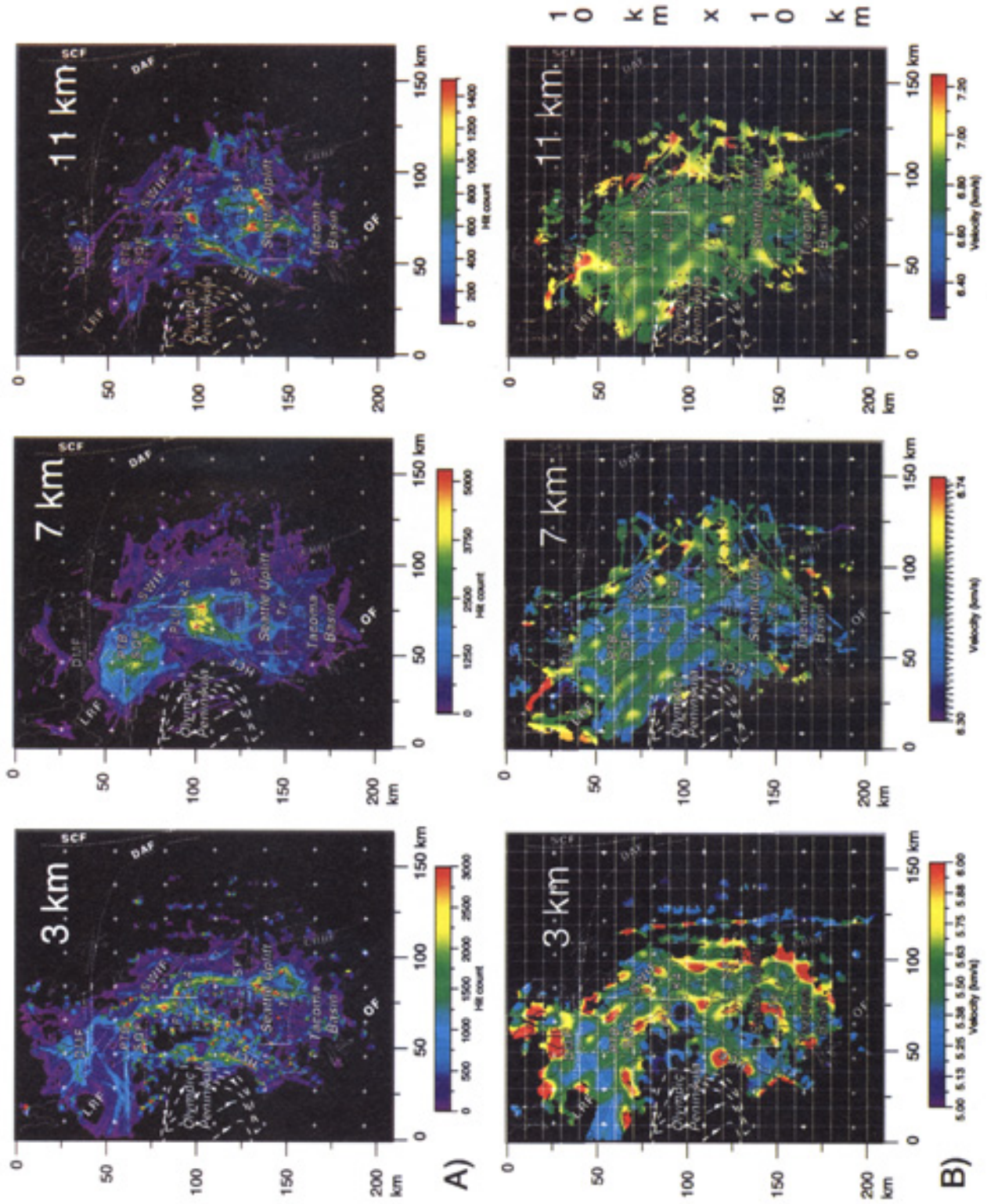
A)
B)
3 km
7 km
11 km
10 km x 10 km
SCF
DAF
LRF
OF
Seattle Uplift
Tacoma Basin
Olympic Peninsula
Hit count
Velocity (km/s)
km

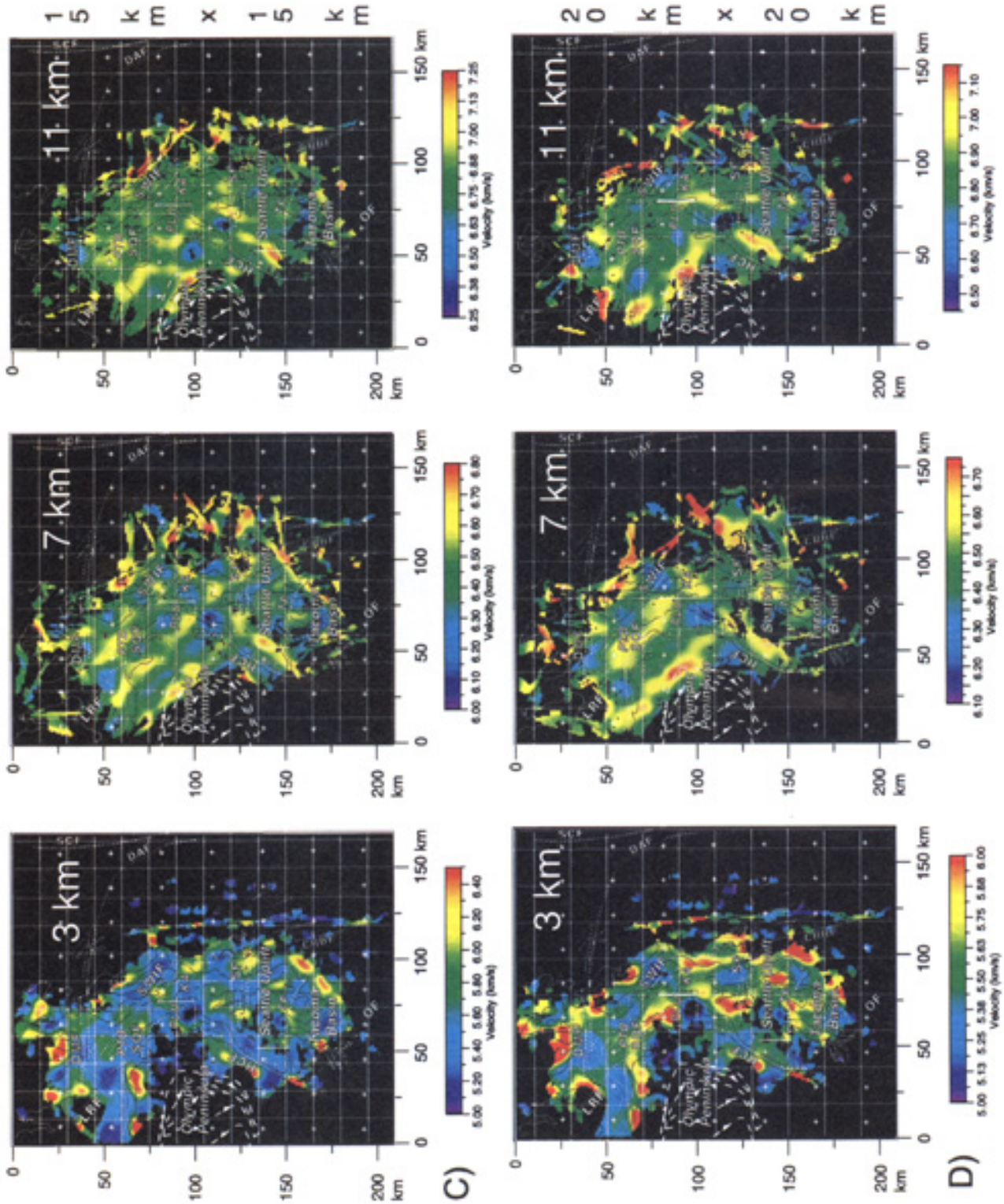
3 km
7 km
11 km
15 km x 15 km
20 km x 20 km
C)
D)
Olympic Peninsula
Seattle Uplift
Tacoma Basin
Velocity (km/s)
0
50
100
150
200 km
150 km

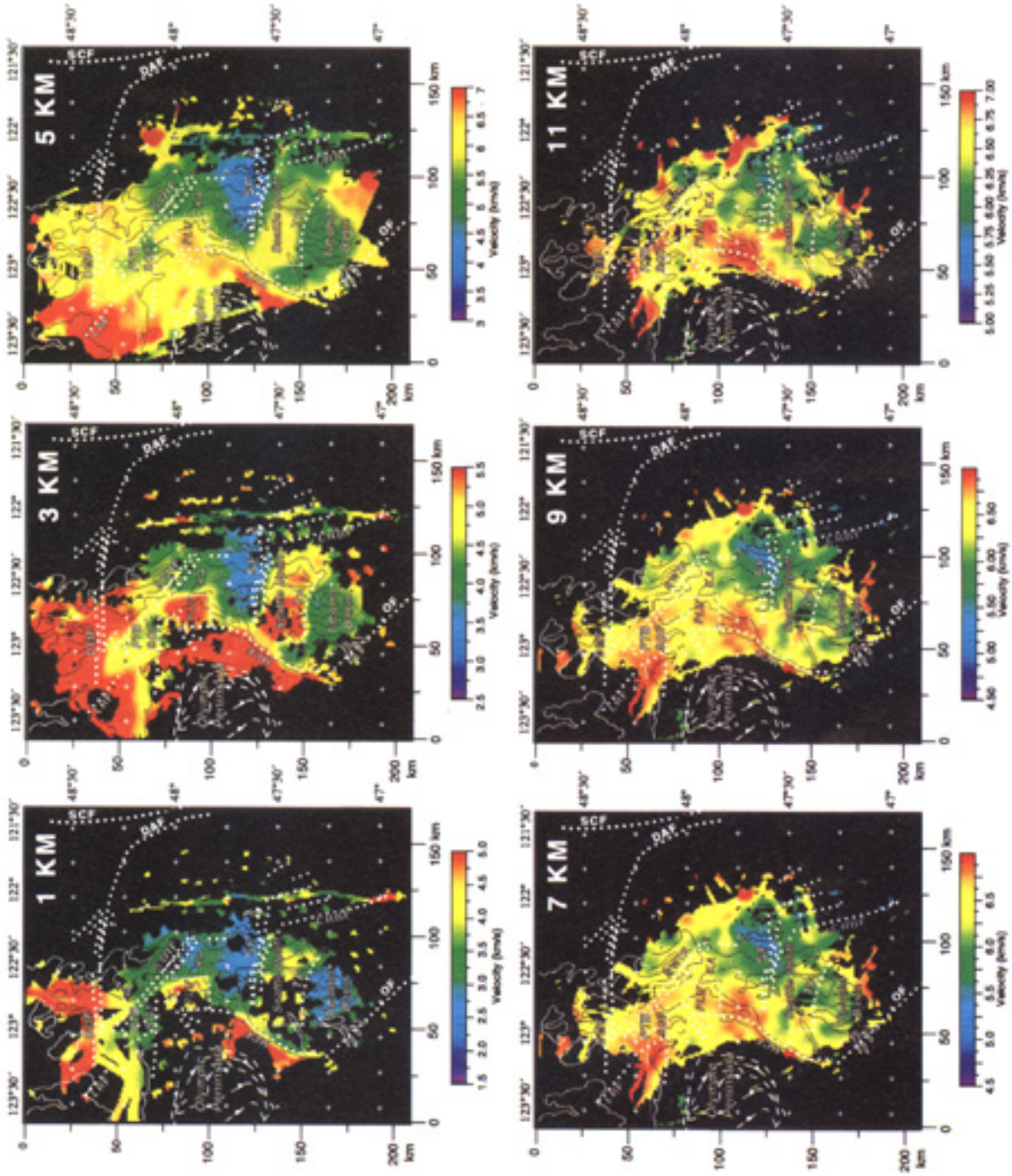

Plate 2. Map views (horizontal slices) of the tomography model at 2 km intervals in depth starting 1 km below sea level. Format is the same as Plate 1. Velocity scale bar differs for each map.

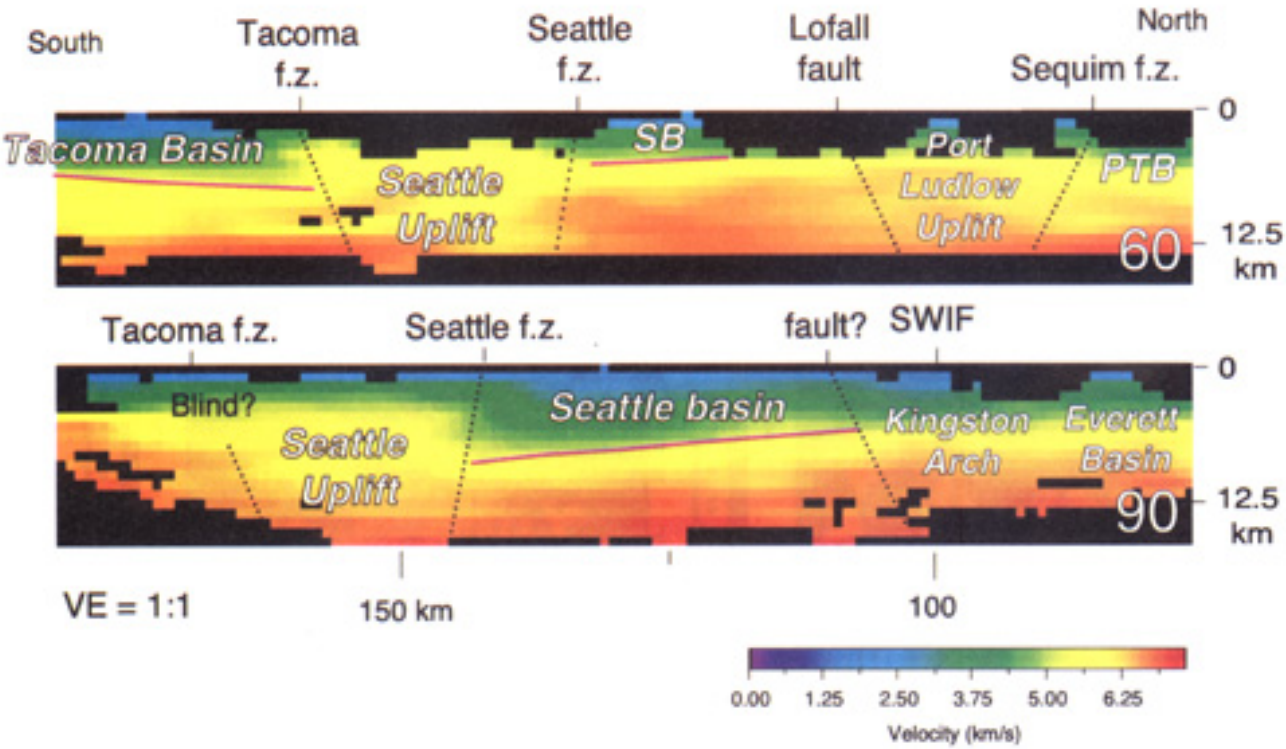

Plate 3. Comparison of north-south cross sections through the SHIPS tomography model at two different locations along the Seattle uplift (given in kilometers from Plate 2). Interpretation of fault dips is schematic (but is consistent with Plate 8). Magenta lines show base of sedimentary basins (picked as the 4.5 km/s contour).

tomography does an excellent job of resolving an arcuate series of basins and intervening basement uplifts landward of the Olympic Mountains and beneath the Puget Lowland (Plate 2). At these depths the basin shapes correlate well with those inferred from gravity and the few deep wells. Basin margins are marked by sharp velocity gradients that correspond to (1) known faults (e.g., the Seattle fault), (2) faults inferred from potential field data (Hood Canal fault [*Gower et al.*, 1985]), and (3) faults imaged on seismic reflection profiling (southern Whidbey Island and Devils Mountain fault zones [*Johnson et al.*, 1996; 2001]). Portions of the Devils Mountain and southern Whidbey Island fault zones are not well resolved by the tomography and apparently lack velocity contrasts, either because they have <1 km of vertical structural relief or because the fault zones juxtapose rocks having similar velocities.

At 5 km depth the overall pattern differs slightly. A few of the E-W velocity anomalies bounding the uplifts in the upper 3 km become less prominent (Plate 2). In their place, a broad swath of relatively low velocities may be traced continuously northward along the center of the lowland from the Olympia fault to just south of the Devils Mountain fault.

Although the horizontal resolution of the tomography decreases below 5 km, the general pattern observed at 5 km seems to persist with depth (Plate 2). A broad rectangular area of relatively lower velocities, bounded by the Olympia and southern Whidbey Island fault zones, is observed. Low velocities associated with the Seattle basin extend to 11 km depth and are bounded northeast of Lakes Washington and Sammamish by a NW trending high-velocity unit. High-velocity roots are imaged in Crescent basement rocks beneath the Seattle uplift, probably reflecting mafic units, basalts, gabbros, and so forth. The triangular-shaped low-velocity anomaly near Port Townsend is no longer seen at or below 7 km. In sections 5.2 to 5.15 we look in greater detail at the major structures in the tomography model in order from south to north.

On the basis of the industry sonic logs (Figure 4) [*Brocher and Ruebel*, 1998] we select the 4.5 km/s contour as representing the top of the Crescent Formation basalt within the deeper basins. Where Crescent Formation basalt shoals or outcrops, we expect its seismic velocity to be lowered as the result of increased fracturing and weathering.

5.1. Inverse Gravity Model of Basin Geometry

In addition to the images of the Cenozoic basin geometry based on the SHIPS tomography model described below, we investigated the three-dimensional geometry of these basins using gravity inversions (Plate 7). For the inversions we used the SHIPS seismic data and other information to constrain a direct calculation of the shape of the basement surface. As defined here, the "basement" surface is the interface between Eocene volcanic rocks and overlying, younger, low-density sedimentary rocks. Inclusion of the Tacoma basin in this inversion lies outside the scope of this paper.

The inverse method [*Jachens and Moring*, 1990] is especially applicable to basins filled with low-density deposits. This iterative method strives to separate the observed gravity field into two components: one produced by low-density basin fill and the other produced by the underlying basement. The basement density is allowed to vary horizontally, whereas the basin fill is forced to follow a specified 1-D density-depth profile. The

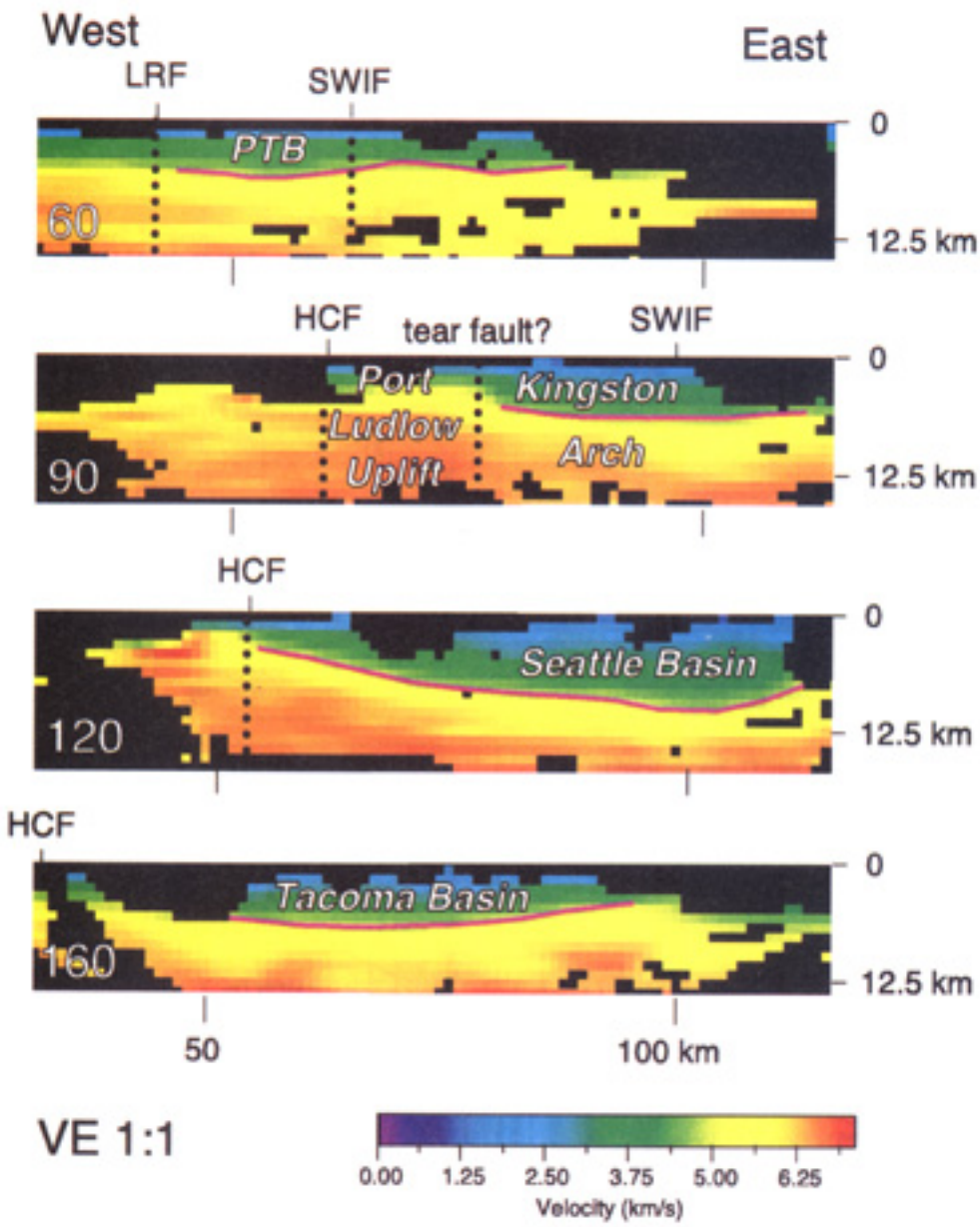

Plate 4. Comparison of east-west cross sections through the SHIPS tomography model at four different locations. Format is that of Plate 3. Fault dips are schematic.

method, as modified by B. A. Chuchel and R. C. Jachens (written communication, 1999), allows for input of well and seismic data to constrain the basin shape.

We assumed that basement crops out in the west as Eocene Crescent Formation, in the north as pre-Tertiary ultramafic rocks, and in the east as Eocene volcanic rocks. The inverse calculation was constrained to fit the depth of Crescent Formation as encountered in deep wells [*Brocher and Ruebel*, 1998] and as interpreted from SHIPS seismic reflection data by *Molzer et al.* [1999]. Table 1 shows the density-depth profile assumed for overlying basin-filling sediments. These densities were estimated from published travel time data [*Johnson et al.*, 1994; *Brocher and Ruebel*, 1998], then converted to density using (1) [*Gardner et al.*, 1974].

$$\rho = 1740\, v^{1/4}, \qquad (1)$$

where ρ, density, and v, seismic velocity, have units of kg/m^3 and km/s, respectively.

In Appendix A we quantitatively compare the tomography results to the observed gravity anomalies using forward calculations of the gravity field based on the tomography model. The tomography model predicts the gravity remarkably well, increasing our confidence that the tomography model has resolved the key features of the shallow crustal structure of the lowland.

5.2. Tacoma Basin

Previous interpretations of the Tacoma basin have been limited to qualitative interpretations of the gravity anomalies [*Gower et al.*, 1985] and seismic reflection lines through it within Puget Sound [*Pratt et al.*, 1997]. The basin is bounded on the

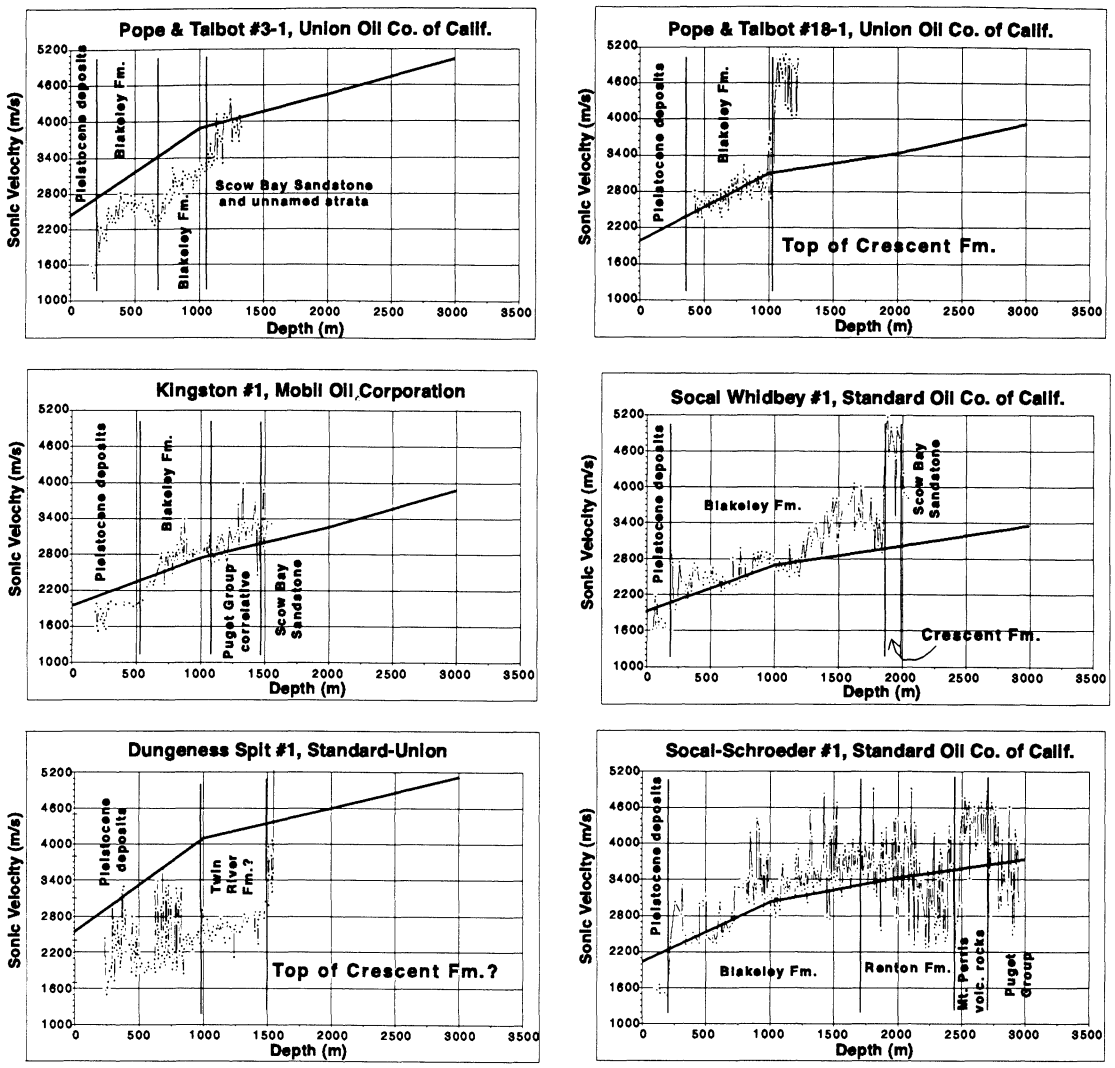

Figure 4. Comparison of tomography results with sonic log data and lithologies for six boreholes [*Brocher and Ruebel*, 1998]. Borehole locations are shown in Figure 2.

north by the Seattle Uplift, on the south by the Black Hills, on the west by the Olympic Mountains, and on the southeast by the Cascade Range (Figure 1).

SHIPS data reveal that Tacoma basin trends ESE-WNW and is ~50 km long and 35-40 km wide (Plates 2-4 and 6). The inferred Olympia fault zone [*Gower et al.*, 1985] along the southwest margin of the basin is not within the region of ray coverage for the 1998 SHIPS tomography. Steep velocity gradients along the basin margin are coincident with structures along Hood Canal and the south side of the Seattle uplift previously inferred to be faults or folds from gravity data ([*Gower et al*, 1985]; see section 5.6). A previously unrecognized NE trending high velocity block defines the SE margin of the basin. This block is oriented subparallel to the margin of the sound, persists to a depth of 9 km, and gives the basin a rhombic shape at depth (Plate 2). This block may be an older, buried structure between the basin and Cascade arc rocks to the southeast, although its coincidence with the margin of the modern sound warrants further study.

SHIPS tomography results show that in cross section the western part of the Tacoma basin is asymmetric, deepening northward. The basin attains a maximum thickness of 6-7 km along the southern boundary of the steep velocity gradient associated with the Seattle uplift (Plate 3, especially kilometer 60). The basin floor is concave in E-W section (kilometer 160 on Plate 4). This concavity and northward thickening contrasts with reflection profiles showing that the basin floor is flat beneath Puget Sound [*Pratt et al.*, 1997].

5.3. Hood Canal Fault Zone

The Hood Canal fault (Figure 1) was previously inferred from the major break in topography and gravity anomalies along Hood Canal [*Gower et al.*, 1985; *Johnson et al.*, 1994]. Rather than precisely following the Hood Canal in map view, however, velocity anomalies in the SHIPS tomography model define a series of segments having N-S and NE-SW trends (Plate 6), that generally track the previously proposed location of the Hood Canal fault zone (Figure 1). Along the western ends of the Tacoma and Seattle basins the basin-bounding velocity anomalies appear to trend nearly N-S. Along the NW corner of the Seattle uplift the anomalies trend NE-SW. A weak velocity low at the edge of the tomography model defines a N-S trend along the western end of the Port Ludlow uplift in a previously proposed location for the Hood Canal fault (Figure 1 and Plate 6) [*Johnson et al.*, 1994].

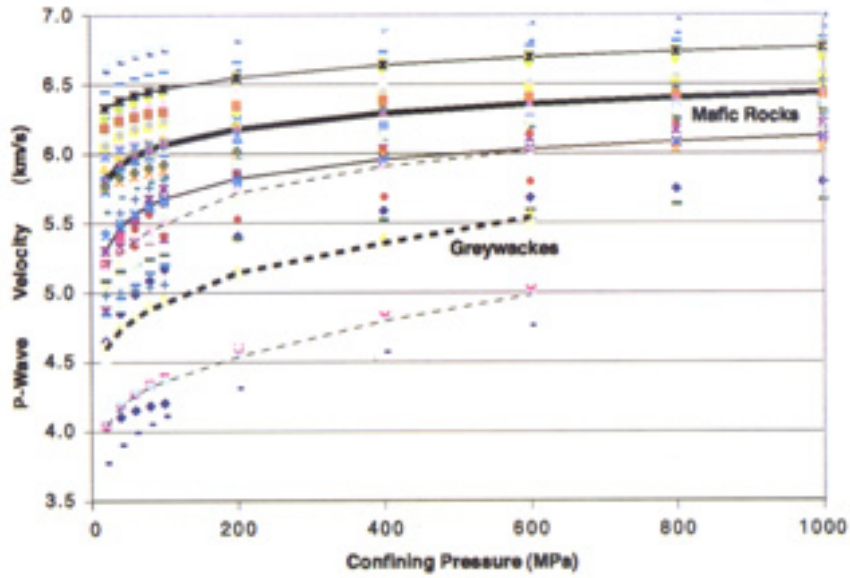

Plate 5. Comparison of laboratory measurements of *P* wave velocity versus confining pressure for 29 mafic volcanic rocks of the Crescent Formation and 11 greywackes from the Olympic Peninsula. Thick solid and dashed lines show the average *P* wave velocity versus confining pressure for each suite of samples. The thinner solid and dashed lines show the first standard deviation from the average values. Different symbols show values for each sample. Sample locations are shown in Figure 1.

In addition to a component of down to the east motion, the sense of displacement on the Hood Canal fault may include strike-slip motion accommodating relative motion between the Olympics and Puget Lowland [*Johnson et al.*, 1994]. Previous tomography models suggested that the topographically high volcanic rocks in the Crescent Formation forming the eastern range front of the Olympic Mountains are faulted down on the east along the Hood Canal fault [*Symons*, 1998; *Parsons et al.*, 1999; *Stanley et al.*, 1999]. Owing to their proximity to the previously proposed Hood Canal fault and their down to the east geometry (e.g., kilometer 120 on Plate 4) we interpret the velocity anomalies in the tomography as representing the Hood Canal fault zone (Plate 6).

5.4. Tacoma Fault Zone

The northern boundary of the Tacoma basin lies along an arcuate structure stretching ~50 km from just north of Tacoma to the western side of the Kitsap Peninsula. The arcuate shape of the structure is defined as the southern boundary of highs in the tomography (Plate 6), gravity (Plate 7a), and aeromagnetic data [*Blakely et al.*, 1999]. The structure, which juxtaposes Eocene Crescent Formation volcanics against younger Tertiary sedimentary rocks, is abruptly truncated by a different N-S trending structure just west of Lynch Cove on the western side of the Kitsap Peninsula (Plate 6). Because this very unusual geometry is also observed in the gravity (Plate 7a) and aeromagnetic data [*Blakely et al.*, 1999], we are confident that this N-S trending structure is real. We are uncertain, however, of its origin. One interpretation is that it represents an N-S trending tear fault.

Gower et al. [1985] interpreted the arcuate structure defined by gravity and aeromagnetic anomalies as a fault or a steep monoclinal fold, down to the south. Using seismic reflection profiles beneath the Puget Sound, *Pratt et al.* [1997] interpreted this structure as the back limb of a fault-propagation fold caused by the Seattle fault zone with as much as 2 km of up to the north structural relief. The structure is not obvious in the N-S cross section through the tomography model at Tacoma (see kilometer 90 of Plate 3). The SHIPS tomography, however, indicates that the inferred relief on the structure increases and the Tacoma basin deepens westward from Puget Sound by several kilometers (compare kilometers 60 and 90 of Plate 3). For this reason and others presented in section 6, we informally refer to this arcuate structure as the Tacoma fault zone. We cannot determine from the tomography whether this structure represents a Holocene fault zone. Evidence that it may be include observations of abrupt Holocene uplift located north of the structure [*Bucknam et al.*, 1992].

Table 1. Density-Depth Profile for Sediments Within the Seattle Basin[a]

Depth Range, km	Density, kg/m^3	Density Contrast, kg/m^3
0.0—1.5	2260	–660
1.5—2.5	2360	–560
2.5—3.5	2420	–500
3.5—4.5	2470	–450
4.5—5.5	2510	–410
> 5.5	2610	–310

[a]The density contrast is relative to the Crescent Formation (density of 2920 kg/m^3).

5.5. Seattle Fault Zone

The northern boundary between the higher velocities associated with the Seattle uplift and lower velocities associated with the Seattle basin (Plate 6) closely matches the location and shape of the complex Seattle fault zone inferred from high-resolution seismic reflection data, aeromagnetic data, and outcrop patterns [*Yount and Gower*, 1991; *Johnson et al.*, 1994, 1999; *Nelson et al.*, 1999; R. J. Blakely et al., submitted manuscript,

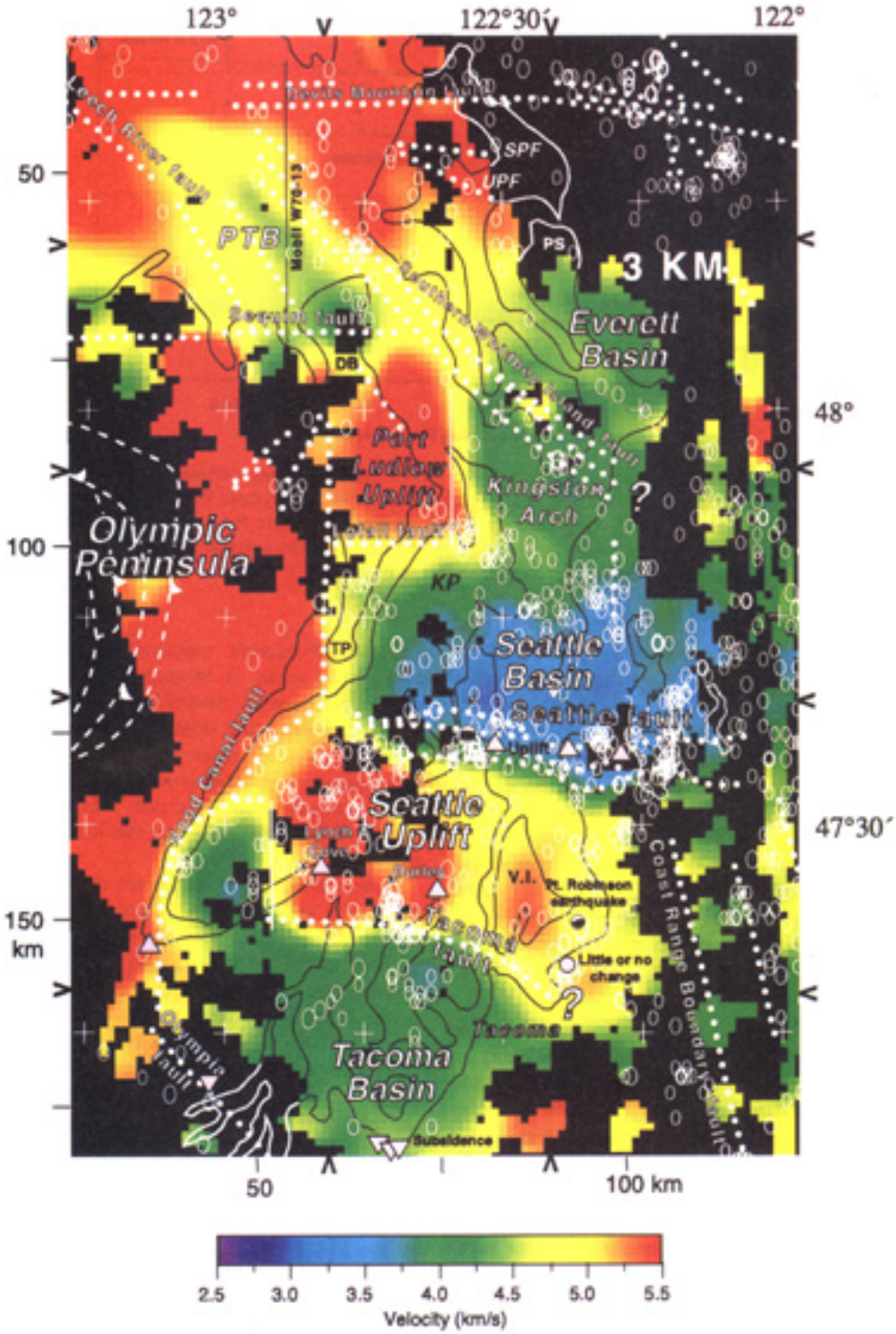

Plate 6. Tomography model for the Tacoma, Seattle, and Port Townsend basins at 3 km depth. Format is identical to that of Plate 2. Arrows show locations of cross sections in Plates 3 and 4. Ellipses show earthquakes, magnitude 2 or greater, since 1970, to a depth of 40 km. Various symbols show sites having evidence of uplift (solid triangles), subsidence (solid inverted triangle), and no vertical motion (filled circle) in an inferred earthquake or earthquakes dated at 1000-1100 years B. P. [*Campbell*, 1981; *Bucknam et al.*, 1992; *Sherrod*, 1998]. DB, Discovery Bay; PS, Port Susan; SPF, Strawberry Point fault; TP, Toandos Peninsula; UPF, Utsulady Point fault.

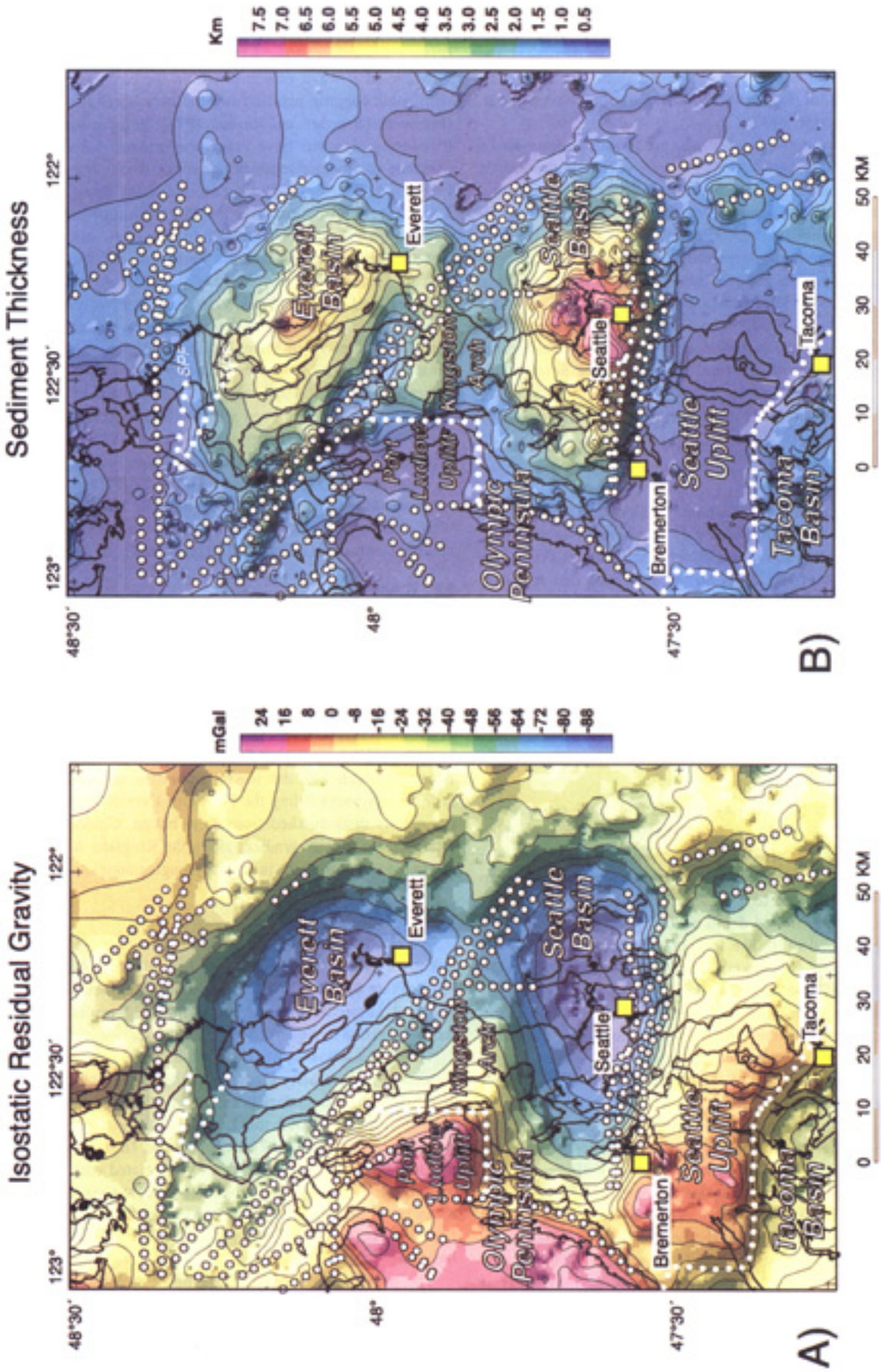

Plate 7. (a) Isostatic residual gravity map of the Puget Lowland. (b) Thickness of Puget Lowland sediments based on inversion of the gravity data. Format is that of Plates 1 and 6.

2000]. The agreement between the geometry of the fault zone inferred from these previous studies and from the strong velocity gradient in the tomography model is striking. In particular, the anomalies in the tomography model also exhibit the southward curvature inferred for the Seattle fault zone by R. J. Blakely et al. (submitted manuscript, 2000).

The SHIPS tomography reveals pronounced along-strike variation in the fault zone. At Redmond and Seattle the Seattle fault zone is associated with a pronounced overhang in seismic velocity consistent with a north vergent thrust fault having 8-9 km of structural relief (Plate 3, kilometer 90). This geometry is compatible with previous interpretations of the Seattle fault zone along this section as a zone of north vergent thrust faulting [*Johnson et al.*, 1994, 1999; *Pratt et al.*, 1997; R. J. Blakely et al., submitted manuscript, 2000]. The SHIPS tomography provides new subsurface information for the western end of the fault zone, showing that the inferred structural relief along the Seattle fault zone diminishes westward to 4-5 km and that the velocity overhang seen near Seattle is not observed at the western end of the fault (kilometer 60 on Plate 3).

5.6. Seattle Uplift

Crescent Formation volcanics crop out along the northwestern portion of the Seattle Uplift (Figure 1) [*Yount and Gower*, 1991; *Haeussler and Clark*, 2000], suggesting the Crescent Formation basalt cores much of the uplift on the west side of the Kitsap Peninsula. The relatively high (6.0-6.8 km/s) seismic velocities determined for the uplift down to 11 km are compatible with laboratory measurements of seismic velocity of the Crescent Formation volcanics (Plates 2-3 and 5). Consistent with higher structural relief along the Tacoma fault zone in the western side of the Kitsap Peninsula, the tomography images higher seismic velocities there than to the north of Tacoma.

5.7. Seattle Basin

The 3-D SHIPS tomography (Plates 2-4) and our gravity inversion (Plate 7b) provide new information on the subsurface geometry of the western end of the Seattle basin and the thickness of the entire Seattle basin. Previous studies of the deep basin have been limited to 2-D seismic reflection lines within Puget Sound having limited depth control [*Johnson et al.*, 1994, 1999; *Pratt et al.*, 1997]. The tomography data reveal that the basin is bounded by prominent velocity anomalies on the south along the Seattle fault zone, on the north by large anomalies along the southern margins of the Port Ludlow uplift and Kingston Arch, and on the west by anomalies along the Hood Canal fault (Plate 6). The eastern basin boundary was not imaged by our tomography (Plate 4, kilometer 120). The SHIPS tomography reveals a low-velocity anomaly associated with the basin extending to maximum depths of ~9 km beneath Seattle and Lake Washington and that the basin shoals to the east and west of Seattle (Plate 4). The gravity inversion indicates that the basin is ~60 km long in the east-west direction and 30 km across in the north-south direction (Plate 7b). More recent seismic refraction profiling suggests that the Seattle basin is closer to 70-75 km long in the east-west direction [*Brocher et al.*, 2000].

In N-S cross section the Seattle basin is asymmetrical at Seattle (kilometer 90 in Plate 3), with velocity isocontours deepening to the south toward the Seattle fault. This basin geometry matches the southerly dip of reflections within the basin seen on coincident industry and SHIPS MCS profiles [*Johnson et al.*, 1994; *Pratt et al.*, 1997; *Fisher et al.*, 1999]. In E-W cross section the basin thins by several kilometers to the west toward the Hood Canal fault where it is abruptly terminated (Plate 4, kilometer 120).

Modeled *P* wave velocities within the basin are in agreement with sonic logging results from industry boreholes to the north (Figure 4) [*Brocher and Ruebel*, 1998]. In these logs (Figure 4), Pleistocene deposits have velocities between 1.5 and 2.0 km/s, Miocene to Eocene sedimentary rocks (including the Blakeley Formation, the Renton Formation, the Scow Bay Sandstone, the Twin River Formation, and the Puget Group) have velocities increasing with depth from 2.5 to 4.3 km/s, and interbedded Eocene volcanic units (Crescent Formation and the Mount Perris volcanic rocks) have velocities between 4.0 and 5.2 km/s [*Brocher and Ruebel*, 1998]. Near Seattle, *P* wave velocities are inverted in consequence of the northward vergence of the fault zone (kilometer 90 in Plate 3), placing higher-velocity Crescent Formation rocks over lower-velocity Quaternary and Tertiary sedimentary rocks. Thus, near Seattle the dip of the southern margin of the basin is even steeper than depicted in the gravity inversion (Plate 7b); the gravity inversion is limited to vertical dips and cannot resolve structural overhangs.

At depth, say at 9 km (Plate 2), the SHIPS tomography data suggest that the Seattle basin has a rhombic NE elongation. East-west cross sections indicate that locally, the basin floor may step sharply downward (kilometer 120 on Plate 4).

5.8. Kingston Arch

The Kingston Arch is a structural high [*Pratt et al.*, 1997], but it is not imaged as a relative velocity high in the uppermost several kilometers of the tomography model (Plate 6). The relatively low velocities at shallow depth on the arch are consistent with its 3 km thick sedimentary cover evident in the Pope and Talbot 18-1, Kingston 1, and Socal-Schroeder 1 boreholes (Figure 4). At shallow depth (e.g., Plate 6), the Kingston Arch has the lower velocities associated with the sedimentary rocks filling the Seattle or Everett basins and thus is not readily distinguished from these basins. *Gower et al.* [1985] interpreted a gravity gradient along the Kingston Arch (Plate 7a) as evidence that the arch is an east plunging anticlinal fold.

5.9. Port Ludlow Uplift

We informally use the name Port Ludlow uplift for an uplift of unknown origin located adjacent to and west of the Kingston Arch (Plate 6). The Port Ludlow uplift is associated with high-velocity anomalies consistent with the Crescent Formation basalts exposed in a quarry within the uplift.

The Port Ludlow uplift is bounded on the south and the north by sharp linear velocity gradients in the tomography model (Plate 6). The southern boundary is an unnamed E-W trending structure, here informally named the Lofall fault zone, for the locality where the gravity (Plate 7), aeromagnetic [*Blakely et al.*, 1999], and tomography gradients (Plate 6) associated with the structure are largest. The Lofall fault zone has brought Crescent Formation rocks up to the north. The only evidence that this structure is a fault zone is the linear, steep geophysical gradients that define its location.

The northern boundary of the uplift is formed by an E-W trending fault previously identified but not named by *Johnson et al.* [1996], here informally named the Sequim fault zone for the locality where geophysical gradients are also largest (discussed more fully in section 5.13; see Plate 6). The Sequim fault zone is an up to the south structure [*Johnson et al.*, 1996]. Velocity

anomalies across the Lofall and Sequim fault zones disappear with depth (Plate 2). We attribute this disappearance to the absence of a significant velocity contrast across the fault zones beneath the Seattle and Port Townsend basins.

The eastern margin of the Port Ludlow uplift is abruptly truncated by a N-S trending structure. This eastern boundary is defined by abrupt eastward deepening in the depth to higher velocities in the tomography model (kilometer 90 in Plate 4); similar to that observed along the western end of the Tacoma fault zone but with an opposite sense of movement (eastside down). We believe this geometry is real and not an artifact of the tomography because it is also observed in the gravity (Plate 7a) and aeromagnetic data [*Blakely et al.*, 1999].

5.10. Southern Whidbey Island Fault Zone

The southern Whidbey Island fault zone (Figure 1) was previously inferred from high-resolution seismic reflection data [*Johnson et al.*, 1996]. As along all of the fault zones in Puget Lowland, structural relief inferred from the SHIPS tomography varies significantly along the southern Whidbey Island fault zone. Our tomography results indicate that structural relief on the fault zone is maximized at the northeast corner of the Port Ludlow uplift, where cross sections demonstrate down to the north and east offset across it (Plate 3). Very little structural relief on the fault zone is inferred along the northwestern end of the fault, where it merges with the Devils Mountain fault zone (Plate 6), or along its southeastern end (Figure 1).

The southeastern end of the southern Whidbey Island fault zone lacks a distinctive velocity contrast within the upper few kilometers (Plates 2 and 6). The absence of a velocity anomaly along the upper reaches of the fault zone at this location indicates that the fault zone there does not juxtapose rocks of substantially different seismic velocities.

5.11. Everett Basin

Our gravity inversion (Plate 7b) shows that Everett basin is ~50 km long, 30 km wide, and elongated in the northwesterly direction. The basin is bounded by the Devils Mountain, southern Whidbey Island, and Darrington fault zones (Figure 1). The basin presumably formed as a consequence of the interactions of these fault zones [*Johnson et al.*, 1996]. The basin is asymmetrical, deepening to the south and east. The linear, east striking northern boundary of the Everett basin coincides approximately with the Strawberry Point and Utsulady Point faults which were recently interpreted from outcrops, high-resolution seismic reflection, subsurface water well, and aeromagnetic data (Plate 7) [*Johnson et al.*, 2001]. Like the Seattle basin, the Everett basin has significant basement topography, highlighted by two subbasins, each exceeding 6 km in depth (Plate 7b). Our SHIPS tomography lacked ray coverage within the Everett basin.

5.12. Port Townsend Basin

We informally use the name Port Townsend basin for the 40 km long by 15 km wide velocity low in the SHIPS tomography that is bounded by the convergence of southern Whidbey Island, Leech River, and Devils Mountain-Darrington fault zones in the eastern Strait of Juan de Fuca (Plate 6). The 3-D geometry of this thin basin has not been previously described, perhaps because it lacks a prominent gravity anomaly (Plate 7a).

Most of the Port Townsend basin lies offshore. N-S cross sections of the SHIPS tomography model indicate that the basin is asymmetric, thickening southward. In E-W cross section (Plate 4, kilometer 60) the basin is more symmetric than in N-S cross section. Industry and SHIPS seismic reflection profiles indicate that it reaches a maximum thickness of ~2 km [*Johnson et al.*, 1996]. Vertical smearing of low velocities in this part of the model is more severe than other parts of the model, owing to the absence of ocean bottom receivers in the eastern Strait of Juan de Fuca. This smearing is revealed by the low seismic velocities in the tomography model to a depth of 7 km and in the misfit of the tomography velocities to the Dungeness Spit 1 and Pope and Talbot 3-1 sonic logs (Figure 4). Thus the tomography model significantly overestimates the thickness of the basin (Plate 4, kilometer 60).

5.13. Sequim Fault Zone

Johnson et al. [1996] identified but did not name a zone of south dipping thrust faulting on Mobil seismic reflection line W70-13 (Plate 6) in the location of previously inferred structure. Structural relief on the top of the Crescent Formation across the structure reaches a maximum of 2 km in the vicinity of the Port Townsend basin [*Johnson et al.*, 1996]. Johnson et al.'s thrust fault zone coincided with a structure defined by a E-W trending aeromagnetic high bounding Eocene volcanic rocks to the south and a thick section of Tertiary sedimentary rocks to the north [*Gower et al.*, 1985].

To facilitate discussion, we informally refer to the structure as the Sequim fault zone (Plate 6), because the town of Sequim lies near the prominent geophysical gradients that define it. The prominent velocity anomalies that bound the Port Ludlow uplift to the north and the Port Townsend basin to the south are coincident, within the limits of the resolution of the tomography model, to the Sequim fault zone. The fault has been interpreted as a north side down structure [*Tabor and Cady*, 1978; *Gower et al.*, 1985], and this is the geometry observed in the tomography (e.g., Plate 3, kilometer 60) and aeromagnetic data [*Blakely et al.*, 1999]. Continuity of the tomography and aeromagnetic anomalies along the northern end of the Port Ludlow uplift [*Blakely et al.*, 1999] are consistent with the eastward projection of the Sequim fault zone to the southern Whidbey Island fault zone.

5.14. Devils Mountain Fault Zone

The Devils Mountain fault zone has been previously identified as a potential Holocene fault zone using seismic reflection profiles, water well lithologies, outcrop control, and aeromagnetic data [*Johnson et al.*, 1996; 2001]. In N-S cross sections the tomography model indicates that the north side of the Devils Mountain fault zone is structurally high, consistent with its interpretation as a zone of north dipping, south vergent thrust faulting [*Johnson et al.*, 1996, 2001]. Structural relief on the Devils Mountain fault zone inferred from the tomography model increases westward, reaching a maximum on the north flank of the Port Townsend basin. Industry seismic reflection profiles are also consistent with this inferred westward increase in structural relief [*Johnson et al.*, 2001]. The tomography and gravity inversion (Plate 7b) both suggest that there is relatively thin sedimentary rock cover on the basement rocks on either side of the fault on its eastern end, consistent with the interpretation of high-resolution seismic reflection data [*Johnson et al.*, 2001]. Thus most of the eastern fault zone lacks a velocity anomaly associated with the fault.

5.15. San Juan Islands

The San Juan Islands, the southeastern tip of Vancouver Island, and the eastern Strait of Juan de Fuca west of the Leech River fault are underlain by pre-Tertiary metamorphic, volcanic, and sedimentary rocks (Figure 1) [*Brandon et al.*, 1988; *Monger*, 1991]. As expected, these regions are all associated with relatively high velocities at all depths in the tomography model (Plate 2). This relationship can be most clearly seen in Plate 6.

6. Discussion

The strength of the tomography model is that it allows us to map upper crustal structures in three dimensions, to examine their spatial variability, and to determine how the structures may relate in the subsurface. The tomography model, however, does not provide information on the recency of the deformation that produced the structure. It is possible that the faults identified here represent old, inactive structures. In the following, we relate the prominent velocity anomalies observed in the SHIPS tomography and large gravity anomalies to seismicity and paleoseismic observations to investigate whether any of these crustal structures might be capable of producing large Holocene earthquakes.

Correlation between paleoseismic evidence for the timing of deformation and the tomography model are limited by the coarse resolution of the tomography relative to the paleoseismic observations. Although it is possible to identify broad structural zones from the tomography, it is not possible to resolve individual faults or fault strands in these images. Thus the paleoseismic evidence can only provide evidence that a broad structural zone may have produced large magnitude Holocene earthquakes. Clearly, the greatest function of these tomographic images is to highlight areas that deserve future detailed geophysical and seismicity studies and to place these small-scale and high-resolution studies into a regional context.

There are similar problems in correlating the microseismicity to fault zones inferred from the tomography. In addition, most of the earthquakes occur 15-30 km deep, whereas the tomography model presented here extends at most to 11 km and is best resolved between 3 and 7 km. Thus, because we have no tomography images of the fault zones below these depths, it is not possible to make a definitive correlation between the structures inferred from the tomography model and most of the microseismicity. Nonetheless, there are a few places in the crust of the Puget Lowland where microseismicity can be traced upward toward the surface from its concentration at 15-30 km. As we will show, these few locations coincide with the large structures imaged by the tomography.

To investigate possible relationships between the microseismicity and the Seattle and Tacoma fault zones, we plotted the microseismicity in Plate 6 and prepared a N-S cross section of the seismicity along Puget Lowland (Plate 8). For the cross section we selected earthquakes from the Pacific Northwest Seismic Network (PNSN) catalog, magnitude 2 or greater, using 40 km wide rectangles that stepped east to the north to avoid microseismicity associated with the Olympics or Cascades (Figure 2). The earthquakes were projected E-W onto the cross section shown in Plate 8, which works best for the E-W trending structures, such as the Seattle fault zone, Kingston Arch, and Devils Mountains fault zone, but smears out the microseismicity for oblique-trending structures (e.g., Tacoma and southern Whidbey Island fault zones). Our cross section resembles that published by *Pratt et al.* [1997] but includes microseismicity through 1999. In Plate 8 we also show focal mechanisms for the 1995 M=5 Point Robinson earthquake [*Dewberry and Crosson*, 1996] and the 1997 M=5 Bremerton earthquake [*Weaver et al.*, 1999]; these represent the largest crustal earthquakes recorded by the PNSN. On Plate 8 the base of the microseismicity at a depth of ~30 km is identified as the bottom of the Crescent Formation basalts imaged by regional seismic tomography [*Stanley et al.*, 1999; *Crosson et al.*, 2000].

6.1. Is the Tacoma Structure a Holocene Fault Zone?

The Tacoma fault zone is one of the most striking geophysical anomalies in the Puget Lowland. Additionally, the Tacoma fault zone is one of the few places in Puget Lowland, the Seattle fault zone being another, where seismicity occurs vertically throughout the upper crust (Plate 8). However, is the Tacoma fault zone a Holocene structure? In our view, the best evidence for Holocene earthquake activity along the Tacoma fault zone is the correlation of the systematic westward increase in the amount of vertical uplift during the AD 784-983 event north of the fault zone [*Bucknam et al.*, 1992; *Sherrod*, 1998] with the westward increase in structural relief inferred from the tomography.

The two sites providing paleoseismic evidence for vertical uplift at AD 784-983 (Lynch Cove and Burley, Plate 6) are located along the western end of the Tacoma fault zone too far south of the Seattle fault zone to record vertical motion along that fault zone [*Bucknam et al.*, 1992; *Sherrod*, 1998]. The uplift at these two sites, however, can be reasonably explained by south vergent thrusting along a wide Tacoma fault zone. (We suggest that the width of the Tacoma fault zone might be comparable to the 8 km width of the Seattle fault zone.) At Lynch Cove a marsh tidal flat was uplifted >3 m at about AD 784-983 [*Bucknam et al.*, 1992] (Plate 6) where we infer the largest amount (6-7 km) of structural relief along the fault zone (Plate 3, kilometer 60). At Burley, uplift could be observed but not quantified [*Bucknam et al.*, 1992], where less structural relief on the fault zone is inferred. To the east, northeast of Tacoma, *Sherrod* [1998] reported little or no evidence for vertical uplift (Plate 6), where the tomography model (Plate 3, kilometer 90) and seismic reflection profiles indicate that the fault zone has a structural relief of about 2 km and that the fault is blind [*Pratt et al.*, 1997]. Thus both the location and the westward increase in the measured Holocene uplift north of the structure suggest to us that identifying the Tacoma structure as a fault zone is warranted, but we fully agree that much more work is needed to document its Holocene earthquake activity and to locate individual fault strands within it.

6.2. Linkage of the Seattle and Tacoma Fault Zones by the Seattle Uplift

Perhaps the most important result of our work is evidence for significant along-strike variation in the inferred structural relief of the Seattle, Tacoma, and other crustal fault zones based on the inferred depth to the top of the Crescent Formation basalts. N-S cross sections through the Seattle uplift show that relief decreases by several kilometers from east to west along the Seattle fault zone but increases by several kilometers from east to west along our inferred Tacoma fault zone (Plate 3). This relation is also nicely imaged by the cross sections of the Seattle and Tacoma basins (Plate 4, kilometers 120 and 160). This keystone-like geometry suggests that the Seattle uplift is a large pop-up block structure caused by uplift on both the Seattle and Tacoma fault zones (Plate 3).

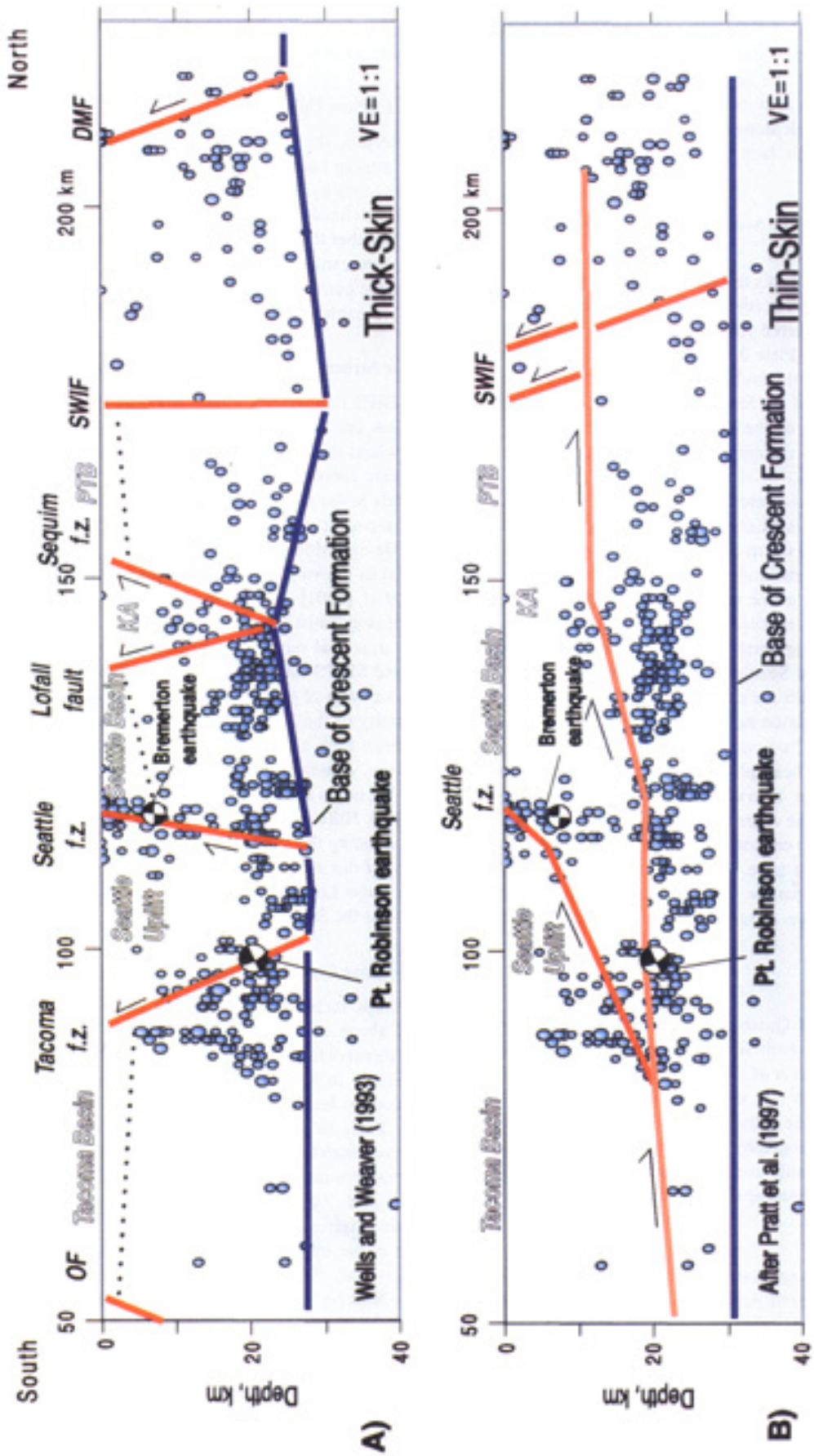

Plate 8. Two models of fault geometry in the Puget Lowland, showing relation of the microseismicity to inferred crustal faults. The 660 hypocenters are from the Pacific Northwest Seismic Network for the years 1970 through 1999 and have magnitude ≥2. The hypocenters were projected E-W along the 40 km wide swath shown in Figure 2. (a) Thick-skinned interpretation based on *Wells and Weaver* [1993], assuming that the faults dip moderately to steeply to the base of the Crescent Formation. (b) Thin-skinned, low-angle detachment interpretation of *Pratt et al.* [1997].

We believe that this geometry indicates that the two fault zones work in concert to accommodate the N-S compression in Puget Lowland. We propose that motion on these fault zones is either directly linked or that motion on one fault can trigger motion on the other because the age of uplift along the Tacoma fault zone at Lynch Cove is identical, within the accuracy of the ^{14}C dating, to the age of uplift along the last major north-directed thrusting event on the Seattle fault zone [*Bucknam et al.*, 1992; *Sherrod*, 1998].

6.3. Downdip Geometry of the Seattle and Tacoma Fault Zones

The seismic tomography lacks the resolution to determine the crustal fault dips at depth. A northward dip of the Tacoma fault zone, however, may be inferred from the northward dip of the floor of the Tacoma basin (Plate 3, kilometer 60). Similarly, a southward dip of the Seattle fault zone is inferred from the southward dip of the floor of the Seattle basin (Plate 3, kilometer 90). However, what is dip of the faults beneath these basins? Currently, we must rely on the microseismicity data to estimate the fault dip below the basins.

Two interpretations of the microseismicity data have been proposed (Plate 8). The thin-skinned, low-angle fault model by *Pratt et al.* [1997] interprets the microseismicity data as evidence that the Seattle fault is a low-angle thrust fault (Plate 8). The thick-skinned interpretation of the microseismicity by *Wells and Weaver* [1993] explains the moderately to steeply dipping zones of microseismicity extending vertically through the crust in the vicinity of the Tacoma and Seattle fault zones as higher angle faults (Plate 8). Both models are consistent with the focal plane of the 1995 M=5 Point Robinson earthquake but in different ways (Plate 8) [*Dewberry and Crosson*, 1996]. *Pratt et al.* [1997] interpret the low-angle focal plane of the Point Robinson earthquake as evidence for a low-angle (25°), south dipping Seattle fault. We note that the alternative focal plane for the Point Robinson earthquake is also consistent with rupture on a steeper, north dipping Tacoma fault zone. We favor the thick-skinned model as being more compatible with our observations of the Tacoma fault zone, but we cannot rule out the thin-skinned model.

6.4. Sequim Fault Zone

Northward thickening of Quaternary units across the Sequim fault zone suggest that the fault zone accommodated significant Quaternary motion [*Johnson et al.*, 1996]. The Sequim fault zone is currently associated with few earthquakes (Plate 6), and its level of Holocene earthquake activity is unknown. On the basis of the continuity of the tomography and aeromagnetic anomalies, we extend the Sequim fault zone eastward to the southern Whidbey Island fault zone, making it at least 50 km long.

6.5. Kingston Arch

Gower et al. [1985] were the first to suggest Quaternary movement along the Kingston Arch on the basis of bedrock at shallow depth. *Pratt et al.* [1997] interpreted the Kingston Arch as either a ramp anticline caused by a 2 km step up in a shallow decollement surface (Plate 8) or for a fault propagation fold above a blind thrust fault. U. S. ten Brink (written communication, 2000) proposed that abrupt offsets of shallow reflections in SHIPS MCS profiles on the Kingston Arch in Puget Sound are evidence for young faulting along the arch. A poorly resolved cloud of deep (10-30 km) microseismicity at the southern margin of the Kingston Arch suggests that this structure may be deforming but do not clearly resolve any shallow crustal faults (Plates 6 and 8).

6.6. Port Ludlow Uplift

We interpret the Port Ludlow uplift as an E-W trending structural pop-up bounded on the south by the Lofall fault zone and on the north by the Sequim fault zone. Although the Lofall fault zone is defined by prominent geophysical anomalies, we are uncertain whether the Lofall fault zone is a fault or of its sense of vergence. Few earthquakes occur within or at the margins of the uplift, and we currently lack any paleoseismic evidence defining the Holocene earthquake history of the Lofall fault.

6.7. Other Structural Uplifts in Puget Lowland

The SHIPS tomography model suggests that the Seattle and Port Ludlow uplifts are only two of several pop-up structures in Puget Lowland that appear to accommodate ~4 mm/yr of north-south forearc compression [*Khazaradze et al.*, 1999]. The San Juan Islands at the northern end of the study area may similarly represent a pop-up structure bounded on the south by the south vergent Devils Mountain fault zone and on the north by structure(s) in the vicinity of the Lummi Island fault (Figure 1). *Johnson et al.* [2001] interpret the Devils Mountain fault zone as a north dipping thrust system, a view compatible with the up to the north structural relief inferred from the tomography model. Industry and SHIPS seismic data from the Strait of Georgia show several kilometers of post mid-Cretaceous relief across structures in the vicinity of the Lummi Island fault consistent with a south dipping thrust fault zone [*Mosher et al.*, 2000; *Zelt et al.*, 2001; S.Y. Johnson, written communication, 2000], making it similar in geometry but not in age to the Seattle fault zone.

The Black Hills form part of a structural high in the southern lowland bounding the southern end of the Tacoma basin [*Gower et al.*, 1985; *Pratt et al.*, 1997]. Thus evidence for structural pop-ups in the Puget Lowland extends from the Black Hills to at least as far north as the San Juan Islands.

6.8. Two-Phase Cenozoic History of the Sedimentary Basins

The abrupt increases in the depth of the basin floor and rhomboid shape of the deepest reaches of the Seattle basin suggest a rhomboidal pull-apart structure. Because this geometry seems unlikely to have resulted from the current N-S directed compression, at least a two-phase history of the basins seems required. Early in their history, the basins apparently formed along approximately N-S trending structures, perhaps during margin-parallel transtension [*Wells et al.*, 1984; *Johnson*, 1985; *Journeay and Morrison*, 1999]. Subsequently, when N-S compression started during the Miocene, as evidenced by beginning of the uplift of the Olympic core complex [*Brandon and Calderwood*, 1990] and the deposition of the middle to late Miocene Blakely Harbor Formation, which was clearly influenced by thrust fault motion along the Seattle fault, the basins have been controlled by E-W trending structures [*Johnson et al.*, 1994; *Pratt et al.*, 1997]. One interpretation is that some of the inferred thrust faults in Puget Lowland represent normal faults now reactivated as reverse faults. Microseismicity beneath the Seattle basin (Plate 6) apparently represents ongoing deformation of the Crescent Formation basement.

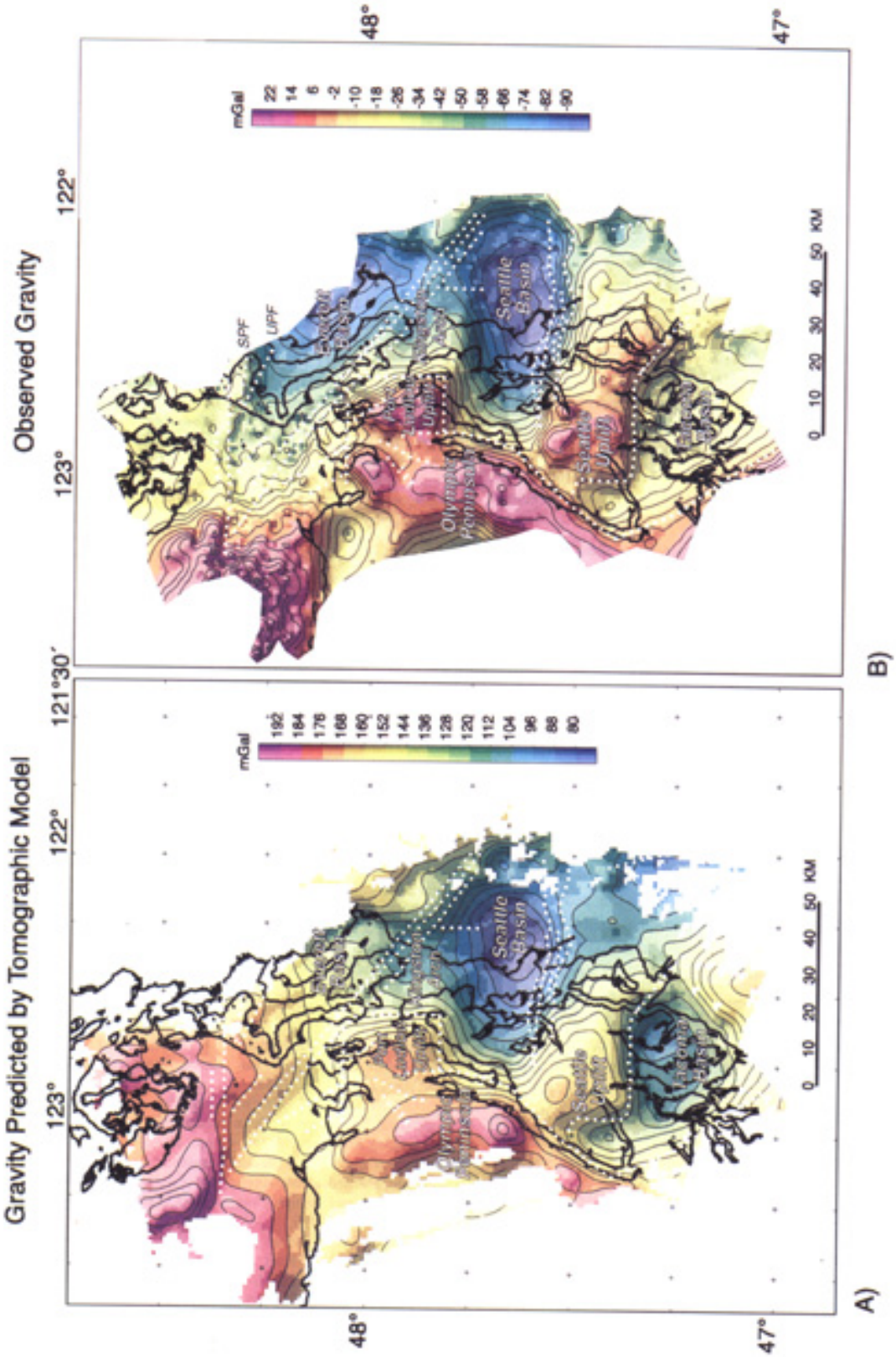

Plate 9. Comparison of observed gravity (Plate 9b) with gravity predicted from seismic velocity model (Plate 9a). Observed and predicted gravity fields are masked in regions of poor seismic ray coverage. Format is the same as Plates 6 and 7.

7. Summary

SHIPS tomography and gravity inversions provide a new tool for imaging the subsurface geometry of crustal uplifts, fault zones, and major Cenozoic basins in the Puget Lowland. Boundaries of the Cenozoic basins and structural uplifts are delineated by prominent velocity and gravity anomaly gradients, in most cases associated with mapped or inferred fault zones. These geophysical gradients present promising targets for future detailed geophysical, seismicity, and paleoseismic investigations to determine the level of Holocene earthquake activity on the structures.

The SHIPS tomography model provides new information on the subsurface geometry of the Seattle and Tacoma fault zones, confirming a newly proposed location for the Seattle fault zone in Seattle (R. J. Blakely et al., submitted manuscript, 2000). Holocene earthquake activity on a broad Tacoma fault zone is suggested by the >3 m of abrupt uplift north of the fault zone at Lynch Cove dated at AD 784-983 [*Bucknam et al.*, 1992]. The subsurface geometry of the Seattle uplift, a basement ridge bounding both the Tacoma and Seattle basins, suggests that it is a large pop-up structure that has been formed by moderate- to high-angle thrusting along the Seattle and Tacoma fault zones. The observed east to west variation in structural relief inferred along both fault zones may result from the transfer of the N-S directed slip from one fault to the other.

SHIPS tomography and seismic reflection data image a number of other structures, including the newly identified Port Ludlow uplift and the Lofall and Sequim fault zones. The Port Ludlow uplift and the San Juan Island uplift and several faults bound the newly identified Port Townsend basin, another of a series of Cenozoic basins in the Puget Lowland.

Appendix A: Forward Gravity Model Based on SHIPS Tomography Model

Although we did not jointly invert the gravity field with the seismic first arrival times, we compared the tomography model to the gravity by converting seismic velocities from the tomographic model (Plate 2) into a three-dimensional density distribution using (1). We assumed that densities within the sedimentary section are given by (1), that Eocene volcanic basement is located wherever seismic velocities exceed 6 km/s, and that the Eocene volcanic basement has a uniform density of 2920 kg/m^3 [*Finn*, 1990]. This assumed basement density closely agrees with the average laboratory measurement of the density of mafic rocks from the Olympic Peninsula (2890 kg/m^3). On the eastern side of the Seattle basin, however, this assumed basement density may overestimate the density contrast between the basin fill and basement rocks of the Cascade Range. We divided the density model into a series of horizontal layers, calculated the gravitational effect of each layer, and summed their various contributions.

Because the seismic tomography and gravity methods are both sensitive to volume averages [*Lees and VanDecar*, 1991], isostatic gravity anomalies predicted from the seismic velocity model compare well with observed isostatic gravity anomalies (Plate 9) in most places, notably at the Seattle basin, Seattle uplift, Port Ludlow uplift, Kingston Arch, Tacoma basin, and exposures of Crescent Formation in the Olympic Peninsula. The computed and observed isostatic gravity anomalies at the Seattle basin show strong similarities in shape, magnitude, and gradient.

The forward gravity model poorly represents the observed gravity over the Everett basin, which lacks seismic ray coverage (Plate 9). The gravity field over the Tacoma basin is not well matched, suggesting that either the tomography did not image the basin well or that the assumed density structure for the basin is incorrect. In addition, the tomographic model predicts a small negative gravity anomaly, centered over the Quimper Peninsula (Figure 1), not present in observed gravity data. The discrepancy between calculated and observed gravity anomalies at the Quimper Peninsula apparently is caused by a zone in the upper 6 km of the crust where densities are higher than predicted from (1).

Acknowledgments. This work was supported by the USGS Marine and Coastal Studies Programs, USGS Seattle Area Natural Hazards Initiative, USGS Venture Capital Fund, and external grants from the USGS National Earthquake Hazards Reduction Program to Oregon State University, the University of Texas El Paso, and the University of Washington. Additional support was given by the Geological Survey of Canada and the U.S. Minerals Management Service. RefTek seismographs were provided by the IRIS/PASSCAL Instrument facility (at Stanford); we thank Marcos Alvarez, Bruce Beaudoin, Russ Sells, and Allan Swisenbank for their support during SHIPS. Tom Burdette organized the fieldwork in the United States. Many individuals helped to deploy the RefTek array and to process the RefTek data. Jon Childs, Guy Cochran, Alan Cooper, and Mike Hamer (USGS) and others served on the *Thompson* science party. We thank NOAA-PMEL for the use of their vessel *SP Hayes* and facilities for USGS OBS operations; we thank Captain Speer, Alvin Buchholtz, Gregory Miller, and Michael Taylor for their support during these operations. We thank the Washington State Departments of Forestry and Parks and Recreation, Olympic National Forest and Park, the Bureau of Land Management, and several smaller parks and public entities for permission to access land under their jurisdiction. We thank the Weyerhaeuser Corp., International Paper Co., and numerous smaller property owners for permission to access their land. We thank Brian Atwater, Bob Forbes, Bob Jachens, Sam Johnson, Alan Nelson, Brian Sherrod, the Associate Editor, and two anonymous reviewers for their thoughtful suggestions on earlier versions of this manuscript.

References

Atwater, B.F., and A.L. Moore, A tsunami about 1000 years ago in Puget Sound, Washington, *Science, 258*, 1614-1617, 1992.

Babcock, R.S., R.F. Burmeister, D.C. Engebretson, and A. Warnock, A rifted margin origin for the Crescent basalts and related rocks in the northern coast range volcanic province, Washington and British Columbia, *J. Geophys. Res., 97*, 6799-6821, 1992.

Blakely, R.J., R.E. Wells, and C.S. Weaver, Puget Sound aeromagnetic maps and data, *U.S. Geol. Surv. Open File Rep., 99-514*, 1999.

Brandon, M.T., and A.R. Calderwood, High-pressure metamorphism and uplift of the Olympic subduction complex, *Geology, 18*, 1252-1255, 1990.

Brandon, M.T., D.S. Cowan, and J.A. Vance, The Late Cretaceous San Juan thrust system, San Juan Islands, Washington, *Spec. Pap. Geol. Soc. Am., 221*, 81 pp., 1988.

Brocher, T.M., and A.L. Ruebel, Compilation of 29 sonic and density logs from 23 oil test wells in western Washington State, *U.S. Geol. Surv. Open File Rep., 98-249*, 41 pp., 1998.

Brocher, T.M., et al., Wide-angle seismic recordings from the 1998 Seismic Hazards Investigation of Puget Sound (SHIPS), western Washington and British Columbia, *U.S. Geol. Surv. Open File Rep., 99-314*, 110 pp., 1999.

Brocher, T.M., et al., Urban seismic experiments investigate the Seattle fault and basin, *Eos Trans. AGU, 81*, 545, 551-552, 2000.

Bucknam, R.C., E. Hemphill-Haley, and E.B. Leopold, Abrupt uplift within the past 1700 years at southern Puget Sound, Washington, *Science, 258*, 1611-1614, 1992.

Bucknam, R.C., B.L. Sherrod, and G. Elendahl, A fault scarp of probable Holocene age in the Seattle fault zone, Bainbridge Island, Washington (abstract), *Seismol. Res. Lett., 70*, 223, 1999.

Campbell, S.K., The Duwamish no. 1 site: A lower Puget Sound shell

midden, Seattle, 564 pp., Univ. Washington, Inst. for Environ. Stud., Office of Public Archaeol., Seattle, 1981.

Christensen, N.I., Compressional wave velocities in rocks at high temperature and pressures, critical thermal gradients and crustal low-velocity zones, *J. Geophys. Res.*, *84*, 6849-6857, 1979.

Christensen, N.I., Measurements of dynamic properties of rock at elevated pressures and temperatures, in *Measurements of Rock Properties at Elevated Pressures and Temperatures*, edited by H. J. Pincus and E. R. Hoskins, pp. 93-107, Am. Soc. for Testing and Mater., Philadelphia, Pa., 1985.

Crosson, R.S., et al., 3-D velocity structure of the Cascadia forearc region from tomographic inversion: Results from full integration of data from multiple active source experiments and earthquake observations, *Eos Trans. AGU*, *81*(48), S71D-01, Fall Meet. Suppl., 2000.

Dewberry, S.R., and R.S. Crosson, The M_D 5.0 earthquake of January 29, 1995 in the Puget Lowland of western Washington: An event on the Seattle fault?, *Bull. Seismol. Soc. Am.*, *86*, 1167-1172, 1996.

Duncan, R.A., A captured island arc chain in the Coast Range of Oregon and Washington, *J. Geophys. Res.*, *87*, 10,827-10,837, 1982.

Finn, C.A., Geophysical constraints on Washington convergent margin structure, *J. Geophys. Res.*, *95*, 19,533-19,546, 1990.

Finn, C.A., W.M. Phillips, and D.L. Williams, Gravity anomaly and terrain maps of Washington, *U.S. Geol. Surv. Geophys. Invest. Map GP-988*, 1991.

Fisher, M.A., et al., Seismic survey probes urban earthquake hazards in Pacific Northwest, *Eos Trans. AGU*, *80* (2), 13, 16-17, 1999.

Gardner, G.H.F., L.W. Gardner, and A.R. Gregory, Formation velocity and density; the diagnostic basics for stratigraphic traps, *Geophysics*, *39*, 770–780, 1974.

Gower, H.D., J.C. Yount, and R.S. Crosson, Seismotectonic map of the Puget Sound region, Washington, *U.S. Geol. Surv. Misc. Invest. Series Map, I-1613*, scale 1:250,000, 1985.

Haeussler, P.J., and K.P. Clark, Preliminary geologic map of the Wildcat lake quadrangle, Kitsap and Mason Counties, Washington, *U.S. Geol. Surv. Open File Rep.*, *00-356*, scale 1:24,000, 2000.

Hole, J.A., Nonlinear high-resolution three-dimensional seismic travel time tomography, *J. Geophys. Res.*, *97*, 6553-6562, 1992.

Hole, J.A., and B.C. Zelt, 3-D finite-difference reflection traveltimes, *Geophys. J. Int.*, *121*, 427-434, 1995.

Humphreys, E., and R.W. Clayton, Adaptation of back projection tomography to seismic travel time problems, *J. Geophys. Res.*, *93*, 1073-1085, 1988.

Jachens, R.C., and B.C. Moring, Maps of the thickness of Cenozoic deposits and the isostatic residual gravity over basement for Nevada, *U.S. Geol. Surv. Open File Rep.*, *90-404*, 15 pp., 2 maps at scale 1:1,000,000, 1990.

Johnson, S.Y., Eocene strike-slip faulting and nonmarine basin formation in Washington, in *Strike-Slip Deformation, Basin Formation, and Sedimentation*, edited by K.T. Biddle and N. Christie-Black, *Spec. Publ. Soc. Econ. Paleontol. and Mineral.*, *37*, 283-302, 1985.

Johnson, S.Y., C.J. Potter, and J.M. Armentrout, Origin and evolution of the Seattle fault and Seattle basin, Washington, *Geology*, *22*, 71-74, 1994.

Johnson, S.Y., C.J. Potter, J.M. Armentrout, J.J. Miller, C. Finn, and C.S. Weaver, The southern Whidbey Island fault, western Washington-An active structure in the Puget Lowland, Washington, *Geol. Soc. Am. Bull.*, *108*, 334-354, and oversized insert, 1996.

Johnson, S.Y., S.V. Dadisman, J.R. Childs, and W.D. Stanley, Active tectonics of the Seattle fault and central Puget Sound, Washington—Implications for earthquake hazards, *Geol. Soc. Am. Bull.*, *111*, 1042-1053, 1999.

Johnson, S.Y., S.V. Dadisman, D.C. Mosher, R.J. Blakely, and J.R. Childs, Late Quaternary tectonics of the Devils Mountain fault and related structures, northern Puget Lowland, *U.S. Geol. Surv. Prof. Pap.*, *1643*, in press, 2001.

Journeay, J.M., and J. Morrison, Field investigation of Cenozoic structures in the northern Cascadia Forearc, southwestern British Columbia, Canada, *Curr. Res. Geol. Surv. Can.*, *1999-A/B*, 239-250, 1999.

Khazaradze, G., A. Qamar, and H. Dragert, Tectonic deformation in western Washington from continuous GPS measurements, *Geophys. Res. Lett.*, *26*, 3153-3156, 1999.

Lees, J.M., and R.S. Crosson, Tomographic imaging of local earthquake delay times for 3-D velocity variation in western Washington, *J. Geophys. Res.*, *95*, 4763-4776, 1990.

Lees, J.M., and J.C. VanDecar, Seismic tomography constrained by Bouguer gravity anomalies: Applications in western Washington, *Pure Appl. Geophys.*, *135*, 31-52, 1991.

Ludwin, R.S., C.S. Weaver, and R.S. Crosson, Seismicity of Washington and Oregon, in *Neotectonics of North America*, edited by D. Burton Slemmons et al., pp. 77-97, Geol. Soc. of Am., Boulder, Colo., 1991.

Massey, N.W.D., Metchosin Igneous Complex, southern Vancouver Island: Ophiolite stratigraphy developed in an emergent island setting, *Geology*, *14*, 602-605, 1986.

McFarland, C.R., Oil and gas exploration in Washington, 1900-1982, *Wash. Div. Geol. Earth Res. Inform. Circ.*, *75*, 119 pp., 1983.

Miller, K.C., G.R. Keller, J.M. Gridley, J.H. Luetgert, W.D. Mooney, and H. Thybo, Crustal structure along the west flank of the Cascades, western Washington, *J. Geophys. Res.*, *102*, 17,857-17,873, 1997.

Miller, M.M., et al., Precise measurements help gauge Pacific Northwest's earthquake potential, *Eos Trans. AGU*, *79*, 269, 275, 1998.

Molzer, P.C., U.S. ten Brink, M.A. Fisher, T.M. Brocher, K.C. Creager, and R.S. Crosson, Seismic structure of Seattle fault, Seattle basin, and Kingston arch, Washington, *Eos Trans. AGU*, *80*(46), Fall Meet. Suppl., F762, 1999.

Monger, J.W.H., Late Mesozoic to Recent evolution of the Georgia Strait-Puget Sound region, British Columbia and Washington, *Wash. Geol.*, *19*, 3-7, 1991.

Moran, S.C., J.M. Lees, and S.D. Malone, *P* wave crustal velocity structure in the greater Mount Rainier area from local earthquake tomography, *J. Geophys. Res.*, *104*, 10,775-10,786, 1999.

Mosher, D.C., and S.Y. Johnson (Eds.), Neotectonics of the eastern Strait of Juan de Fuca; a digital geologic and geophysical atlas, compiled by G.J. Rathwell, R.B. King, and S.B. Rhea, *Geol. Surv. Can. Open File Rep.*, *3931*, 2000.

Mosher, D.C., J.F. Cassidy, C. Lowe, Y. Mi, R.D. Hyndman, G.C. Rogers, and M. Fisher, Neotectonics in the Strait of Georgia: First tentative correlation of seismicity with shallow geological structure in southwestern British Columbia, *Curr. Res. Geol. Surv. Can.*, *2000-A22*, 9 pp., 2000.

Nelson, A.R., S.K. Pezzopane, R.C. Bucknam, R.D. Koehler, C.F. Narwold, H.M. Kelsey, W.T. Laprade, R.E. Wells, and S.Y. Johnson, Holocene surface faulting in the Seattle fault zone, Bainbridge Island, Washington (abstract), *Seismol. Res. Lett.*, *70*, 223, 1999.

Parsons, T., R.E. Wells, M.A. Fisher, E. Flueh, and U.S. ten Brink, Three-dimensional velocity structure of Siletzia and other accreted terranes in the Cascadia forearc of Washington, *J. Geophys. Res.*, *104*, 18,015-18,039, 1999.

Pratt, T.L., S. Johnson, C. Potter, W. Stephenson, and C. Finn, Seismic reflection images beneath Puget Sound, western Washington state: The Puget Lowland thrust sheet hypothesis, *J. Geophys. Res.*, *102*, 27,469-27,489, 1997.

Sherrod, B.L., Late Holocene environments and earthquakes in southern Puget Sound, Ph.D. thesis, 159 pp., Univ. of Wash., Seattle, 1998.

Simpson, R.W., and A. Cox, Paleomagnetic evidence for tectonic rotation of the Oregon Coast Range, *Geology*, *5*, 585-589, 1977.

Snavely, P.D., Jr, and R.W. Wells, Cenozoic evolution of the continental margin of Oregon and Washington, in *Assessing Earthquake Hazards and Reducing Risk in the Pacific Northwest*, edited by A.M. Rogers et al., *U.S. Geol. Surv. Prof. Pap.*, *1560*, 161-182, 1996.

Snavely, P.D., N.S. MacLeod, and H.C. Wagner, Tholeiitic and alkalic basalts of the Eocene Siletz River volcanics, Oregon Coast Range, *Am. J. Sci.*, *266*, 454-481, 1968.

Stanley, D., A. Villasenor, and H. Benz, Subduction zone and crustal dynamics of western Washington: A tectonic model for earthquake hazards evaluation, *U.S. Geol. Surv. Open File Rep.*, *99-311*, 64 pp., 64 illustrations, 1999.

Symons, N., Seismic velocity structure of the Puget Sound region from 3-D non-linear tomography, Ph.D. thesis, 168 pp., Univ. of Wash., Seattle, 1998.

Symons, N.P., and R.S. Crosson, Seismic velocity structure of the Puget Sound region from 3-D non-linear tomography, *Geophys. Res. Lett.*, *24*, 2593-2596, 1997.

Tabor, R.W., and W.M. Cady, Geologic map of the Olympic Peninsula, Washington, *U.S. Geol. Surv. Misc. Invest. Ser. Map, I-994*, two sheets, 1978.

Tréhu, A.M., I. Asudeh, T.M. Brocher, J. Luetgert, W.D. Mooney, J.L. Nabelek, and Y. Nakamura, Crustal architecture of the Cascadia forearc, *Science*, *266*, 237-243, 1994.

Vidale, J.E., Finite-difference calculation of traveltimes in three dimensions, *Geophysics*, *55*, 521-526, 1990.

Weaver, C.S., K. Meagher, R.J. Blakely, and R.E. Wells, The June 23 1997 Bainbridge Island, Washington, earthquake: Evidence that the Seattle fault is seismically active (abstract), *Seismol. Res. Lett.*, *70*, 219-220, 1999.

Wells, R.E., and C.S. Weaver, Block deformation in Puget Lowland, in *Proceedings of the National Earthquake Prediction Evaluation Council*, edited by V.E. Frizzel, *U.S. Geol. Surv. Open File Rep.*, *93-333*, 14-16, 1993.

Wells, R.E., D.C. Engebretson, P.D. Snavely Jr, and R.S. Coe, Cenozoic plate motions and the volcano-tectonic evolution of western Oregon and Washington, *Tectonics*, *3*, 275-294, 1984.

Wells, R.E., C.S. Weaver, and R.J. Blakely, Fore-arc migration in Cascadia and its neotectonic significance, *Geology*, *26*, 759-762, 1998.

Yount, J.C., and H.D. Gower, Bedrock geologic map of the Seattle 30' by 60' quadrangle, Washington, *U.S. Geol. Surv. Open File Rep.*, *91-147*, 37 pp., 5 sheets, scale 1:100,000, 1991.

Zelt, B.C., R.M. Ellis, C.A. Zelt, R.D. Hyndman, C. Lowe, G.D. Spence, and M.A. Fisher, Three-dimensional crustal velocity structure beneath the Strait of Georgia, British Columbia, *Geophys. J. Int.*, *144*, 695-712, 2001.

R. J. Blakely and V. E. Langenheim, U.S. Geological Survey, 345 Middlefield Road, M/S 989, Menlo Park, CA 94025. (blakely@usgs.gov; zulanger@usgs.gov.)

T. M. Brocher, U.S. Geological Survey, 345 Middlefield Road, M/S 977, Menlo Park, CA 94025. (brocher@usgs.gov)

N. I. Christensen, Department of Geology and Geophysics, 1215 W. Dayton St., University of Wisconsin, Madison, WI 53706. (chris@geology.washington.edu)

K. C. Creager, R. S. Crosson, L. A. Preston, and T. Van Wagoner, Department of Earth and Space Sciences, University of Washington, Seattle, WA 98195. (kcc@geophys.washington.edu; bob@geophys.washington.edu; tvan@geophys.washington.edu; preston@geophys.washington.edu.)

M. A. Fisher and T. Parsons, U.S. Geological Survey, 345 Middlefield Road, M/S 999, Menlo Park, CA 94025. (mfisher@usgs.gov; tparsons@usgs.gov.)

R. A. Hyndman, Pacific Geoscience Centre, 860 W. Saanich Road, P.O. Box 6000, Sidney, British Columbia, Canada V8L 4B2. (hyndman@pgc.nrcan.gc.ca)

K. C. Miller and C. M. Snelson, Department of Geological Sciences, University of Texas at El Paso, El Paso, TX 79968. (miller@geo.utep.edu; snelson@geo.utep.edu.)

D. C. Mosher, Geological Survey of Canada-Atlantic, 1 Challenger Dr., P.O. Box 1006, Dartmouth, Nova Scotia, Canada, B2Y 4A2. (mosher@agc.bio.ns.ca)

T. L. Pratt, U.S. Geological Survey, School of Oceanography, University of Washington, Seattle, WA 98195. (tpratt@usgs.gov)

K. Ramachandran and G. D. Spence, School of Earth and Ocean Sciences, University of Victoria, Victoria, British Columbia, Canada V8W 3P6. (kumaran@uvic.ca; gspence@geosun1.seos.uvic.ca.)

N. P. Symons, Sandia National Laboratories, POB 5800 MS-0750, Alburquerque, NM 87185. (npsymon@sandia.gov)

U. S. ten Brink, U.S. Geological Survey, Woods Hole Field Center, 384 Woods Hole Road, Woods Hole, MA 02543. (utenbrink@usgs.gov)

A. M. Tréhu, College of Oceanography, Oregon State University, Oceanography Adminstration Building 104, Corvallis, OR 97331. (trehu@oce.orst.edu)

C. S. Weaver, U. S. Geological Survey, Department of Earth and Space Sciences, University of Washington, Seattle, WA 98195. (craig@usgs.gov)

R. E. Wells, U.S. Geological Survey, 345 Middlefield Road, M/S 975, Menlo Park, CA 94025. (rwells@usgs.gov)

B. C. Zelt, School of Ocean and Earth Science and Technology, University of Hawaii, 1680 East-West Road, Honolulu, HI 96822. (bzelt@akule.soest.hawaii.edu)

(Received July 31, 2000; revised January 11, 2001;
accepted February 22, 2001.)